

Review

Open Access



In-situ transmission electron microscopy shedding light on the mechanical properties of nanoscale materials

Chunmeng Liu^{1,3} , Kemeng Yang¹, Jiaqi Zhang^{1,2} , Shaobo Cheng^{1,2} , Chongxin Shan^{1,2}

¹Henan Key Laboratory of Diamond Optoelectronic Materials and Devices, Key Laboratory of Materials Physics, Ministry of Education, and School of Physics, Zhengzhou University, Zhengzhou 450052, Henan, China.

²Institute of Quantum Materials and Physics, Henan Academy of Sciences, Zhengzhou 450046, Henan, China.

³Center of Advanced Analysis & Gene Sequencing, Zhengzhou University, Zhengzhou 450001, Henan, China.

Correspondence to: Prof. Jiaqi Zhang, Henan Key Laboratory of Diamond Optoelectronic Materials and Devices, Key Laboratory of Materials Physics, Ministry of Education, and School of Physics, Zhengzhou University, No. 100 Science Avenue, Zhengzhou 450052, Henan, China. E-mail: zhangjq@zzu.edu.cn; Prof. Shaobo Cheng, Henan Key Laboratory of Diamond Optoelectronic Materials and Devices, Key Laboratory of Materials Physics, Ministry of Education, and School of Physics, Zhengzhou University, No. 100 Science Avenue, Zhengzhou 450052, Henan, China. E-mail: chengshaobo726@126.com

How to cite this article: Liu C, Yang K, Zhang J, Cheng S, Shan C. *In-situ* transmission electron microscopy shedding light on the mechanical properties of nanoscale materials. *Microstructures* 2024;4:2024055. <https://dx.doi.org/10.20517/microstructures.2023.109>

Received: 31 Dec 2023 **First Decision:** 8 Mar 2024 **Revised:** 24 Mar 2024 **Accepted:** 11 Apr 2024 **Published:** 13 Sep 2024

Academic Editor: Xiaozhou Liao **Copy Editor:** Fangling Lan **Production Editor:** Fangling Lan

Abstract

Characterizing the mechanical properties of nanomaterials (NMs) has always been a challenge for researchers due to their size effect and the difficulty of sample manipulation. In recent years, researchers have integrated scanning tunneling microscopy, atomic force microscopy and other techniques into transmission electron microscopy (TEM); thereby, advanced *in-situ* TEM nanomechanical measurement techniques for NMs have emerged. The study of mechanical properties using *in-situ* TEM allows a direct correlation among mechanical properties, atomic structures, and their dynamic processes. However, systematic reviews on these *in-situ* TEM measurement techniques, their working principles, and the corresponding results obtained by these methods are still limited. This review introduces the basic principles of recently developed *in-situ* TEM techniques (including TEM-atomic force microscopy and TEM-micromechanical systems), the features of these measurement techniques, the research progress in characterizing the mechanical properties and deformation behaviors of NMs by the *in-situ* TEM, and the influence of surface effects and defects on the mechanical properties of NMs. In perspective, several challenges regarding improving the *in-situ* TEM technique and analyzing the *in-situ* TEM data are addressed.

Keywords: Nanomaterials, *in-situ* transmission electron microscopy, mechanical properties, plasticity, Young's modulus



© The Author(s) 2024. **Open Access** This article is licensed under a Creative Commons Attribution 4.0 International License (<https://creativecommons.org/licenses/by/4.0/>), which permits unrestricted use, sharing, adaptation, distribution and reproduction in any medium or format, for any purpose, even commercially, as long as you give appropriate credit to the original author(s) and the source, provide a link to the Creative Commons license, and indicate if changes were made.



INTRODUCTION

Nanomaterials (NMs), as the fundamental building blocks of the future nanoscience and nanotechnology, have attracted much attention^[1-3]. They usually exhibit unique and novel physical and chemical properties such as excellent electrical and thermal conductivity, controllable magnetic, optical and catalytic properties, *etc.*, which endows them promising potentials as nanoscale interconnects and active elements in various applications such as optical electronics and micro/nanoelectromechanical systems (MEMS/NEMS)^[4-15]. Among these physical and chemical attributes, the mechanical characteristics of NMs have attracted particular interest due to the inevitable external forces and deformations during their applications. Furthermore, since these features could be modulated by the strain, understanding the mechanical properties of NMs is crucial for the optimal design, expected performance, and reliability of nanodevices^[16-20]. Due to the ultra-small size and large surface-to-volume ratio of NMs, surface effects and quantum confinement appeared, and thus, the mechanical properties of NMs are much different from their bulk counterparts, and many unexpected behaviors have emerged^[21,22]. The study of nanomechanics has also been one of the hot topics of research.

At early stages, the computational and theoretical approaches were mainly applied to explore the mechanical properties of NMs due to the limitations of the experimental equipment^[23-26]. Although the theoretical result shows that they have unique mechanical properties, this issue remains unclarified. For example, the Young's modulus of face-centered cubic (FCC) metals (e.g., gold (Au) and copper (Cu)) has been reported to increase with decreasing size at 0 K, whereas it declines with size reduction at room temperature^[27]. Molecular-dynamics (MD) simulations and first-principles calculations can predict the NM deformation process by obtaining stress-strain curves; for instance, the transformation of atomic configuration of ultrafine Au nanowires with a cross-section of seven atoms is predicted to be related to the stretching direction during plastic deformation^[28]. However, the calculated results strongly depended on the chosen parameters, such as the exchange-correlation functional or quasi-potentials, thus sometimes inducing contradictory results. For example, Zhou *et al.* investigated the size effect on the Young's modulus of Cu by using a combination of molecular statics and ab initio calculations; however, they obtained the different behaviors when using the different potentials. Specifically, as the size decreases, the materials become stiffer when using embedded atom method (EAM) potential but get softer when choosing the Lennard-Jones potential^[29].

With the continuous development of advanced microscopy techniques, including experiments using scanning tunneling microscopy (STM)^[30], atomic force microscopy (AFM)^[31,32], and scanning electron microscopy (SEM)^[33], experiments have been designed to investigate the special mechanical properties of NMs. Wu *et al.* reported that the Young's modulus of Au nanowires is independent of the diameter when in the range of 40-250 nm using an AFM-based method^[34]. The mechanical properties were measured using a cantilever to bend Au nanowires at the middle, with both ends of the nanowire fixed. Hoffmann *et al.* measured the average strength of silicon (Si) nanowires with diameters between 100 and 200 nm before breaking by integrating an AFM setup inside a SEM, which is 12 GPa (about 6% of the Young's modulus of Si along the nanowire direction)^[35]. Frequency modulation methods have been developed to investigate the mechanical properties of NMs, such as the gradient of force (force constant or so-called spring constant) which can be measured from the shift of the resonance frequency of the force sensor^[36-38]. In addition, a mechanically controllable break junction (MCBJ) system combined with a tuning fork as a force sensor can also be used to investigate the mechanical properties of platinum (Pt) nanocontacts and atomic chains by Shiota *et al.*^[39]. However, obtaining structural information of the NMs, such as the crystal orientation, defect

and atomic arrangement, is challenging for these methods. Therefore, the elucidation of the nanomechanics, which strongly depends on the atomic configurations, is blocked. In addition, the dynamic processes of structural evolution and atomic migration, which are crucial for the plastic deformation and fracture processes of materials, are also difficult to detect with the above methods.

In recent years, *in-situ* transmission electron microscopy (TEM) techniques have attracted much attention due to their ability to easily manipulate NMs and directly observe their mechanical behavior at the atomic level. The advantages of this novel approach allow it to be used to investigate the crystal structure-dependent mechanical properties of materials at the nanoscale and further underlying mechanisms of related devices^[40,41]. Meanwhile, the various modes of *in-situ* nanomechanical testing of NMs, including bending^[42], uniaxial loading^[43], nanoindentation^[44], *etc.*, have been developed. Although NMs possess small sizes, the *in-situ* TEM technique has shown its advantages in establishing their property-structure relationships from their basic behaviors to atomic-level mechanisms. Figure 1 illustrates the *in-situ* TEM methods including TEM-STM, TEM-AFM, strain devices, MEMS, and nanoindentation & gripper^[45-50], which are used to study the mechanical properties and the main research targets such as the elasticity, plasticity and friction of the NMs^[47,48,51-54].

In this review, we will survey the recent advanced research progress on the mechanical properties of NMs using *in-situ* TEM methods. Section "TECHNIQUES FOR *in-SITU* NANOMECHANICAL MEASUREMENT" describes the basic principles of different *in-situ* TEM mechanical testing techniques and their characteristics in measuring nanomechanics. Section "MECHANICAL PROPERTIES OF NANOMATERIALS" reviews the main mechanical properties and behaviors of NMs that can be studied using the above mentioned *in-situ* TEM techniques. Section "FACTORS INFLUENCING THE MECHANICAL PROPERTIES OF NANOMATERIALS" summarizes the factors affecting the mechanical properties of NMs such as surface effects and defects. Section "SUMMARY AND OUTLOOK" provides a brief summary and outlook on future research directions.

TECHNIQUES FOR *IN-SITU* NANOMECHANICAL MEASUREMENT

With the rapid development of experimental instruments, people have begun to explore the mechanical properties of NMs based on new testing techniques. Various measurement instruments, such as STM, AFM, MEMS, *etc.*, have been integrated into TEM sample holders. The suitability of different techniques was organized in Table 1, and the detailed information such as the advantages and limitations of the related techniques for the mechanical measurement of NMs are introduced later.

TEM-STM

As shown in Figure 2A, STM^[55] is an instrument based on the tunneling effect between an atomically sharp metal tip and a sample surface, which can record images from 100 pm to a few nanometers. A metal tip, whose position was adjusted by a piezoelectric actuator, was scanned across the sample surface. A feedback loop adjusted the voltage applied to the piezoelectric actuator to keep the tunneling current constant and record the height to obtain the image. Researchers incorporated the STM probes and piezoelectric actuators into the TEM holders for studying the mechanical properties of NMs. Since the position of the STM probe can be precisely controlled by the piezoelectric ceramics down to the picometer scale, it is possible to deform the material by compression, bending, *etc.*, with the STM probe. The material structure during deformation is analyzed with TEM images or diffraction patterns. In addition, since a current can be applied to the sample through the STM probe, the TEM-STM technique can also be used to analyze the relationship between the electrical or electromechanical properties of a material.

Table 1. The introduction of various in-situ TEM methods in major mechanical loading mode, advantage and disadvantages, suitable sample size, and major study target

<i>In-situ</i> TEM method	Major loading mode	Advantages and disadvantages	Suitable sample size	Major study target
TEM-STM	Tensile, compress, shear, complex loading	Simple sample preparation, multiple loading methods, <i>cannot obtain force signal, difficulty in tilting the sample</i>	From a few nanometers to several hundred nanometers	Plastic properties
TEM-AFM	Tensile, compress, shear, complex loading	Multiple loading methods, could obtain force signal, <i>difficulty in tilting the sample, data analysis difficulty</i>	From a few nanometers to several hundred nanometers	Plastic properties Elastic properties
Strain device	Tensile	Simple sample preparation, double tilt, <i>less loading mode, cannot obtain force signal</i>	From tens nanometers to micrometers	Plastic properties
TEM-MEMS	Tensile, compress, shear, complex loading	Multiple loading methods, could obtain force signal, double tilt, <i>complex sample preparation</i>	From hundreds of nanometers to micrometers	Plastic properties Elastic properties
Nanoindentation & tensile gripper	Tensile, compress	Simple sample preparation, could obtain force signal, <i>less loading mode, difficulty in tilting the sample</i>	From hundreds of nanometers to micrometers	Plastic properties Elastic properties

Note: the italic and bold fonts in the table reveal the disadvantages of various *in-situ* TEM methods.

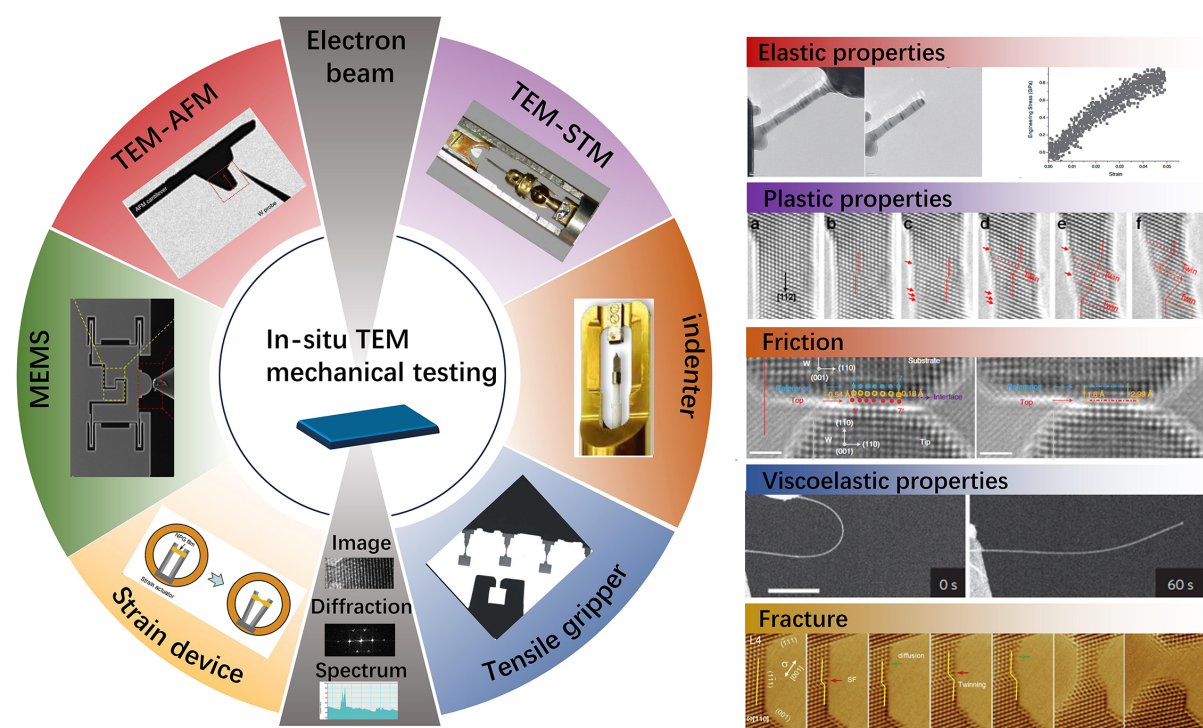


Figure 1. Current advanced *in-situ* TEM nanomechanical testing setups include TEM-STM, TEM-AFM, strain device, MEMS, and nanoindentation & gripper^[45-50]. The main research targets such as the elasticity, plasticity and friction of the NMs could be performed using the above methods^[48,51-54]. Reproduced with permission from 2011 ACS publications^[45], 2021 Springer Nature^[46], 2021 The American Association for the Advancement of Science^[47], 2019 Elsevier^[48], 2011 ACS publications^[49], 2016 Elsevier^[50], 2011 Wiley-VCH GmbH^[51], 2019 ACS publications^[52], 2022 Springer Nature^[53], and 2015 Springer Nature^[54].

To facilitate sample mounting, the movement of the STM probe usually consists of a coarse motion part and a fine motion part. Figure 2B shows a common design of the TEM-STM holder, which consists of a

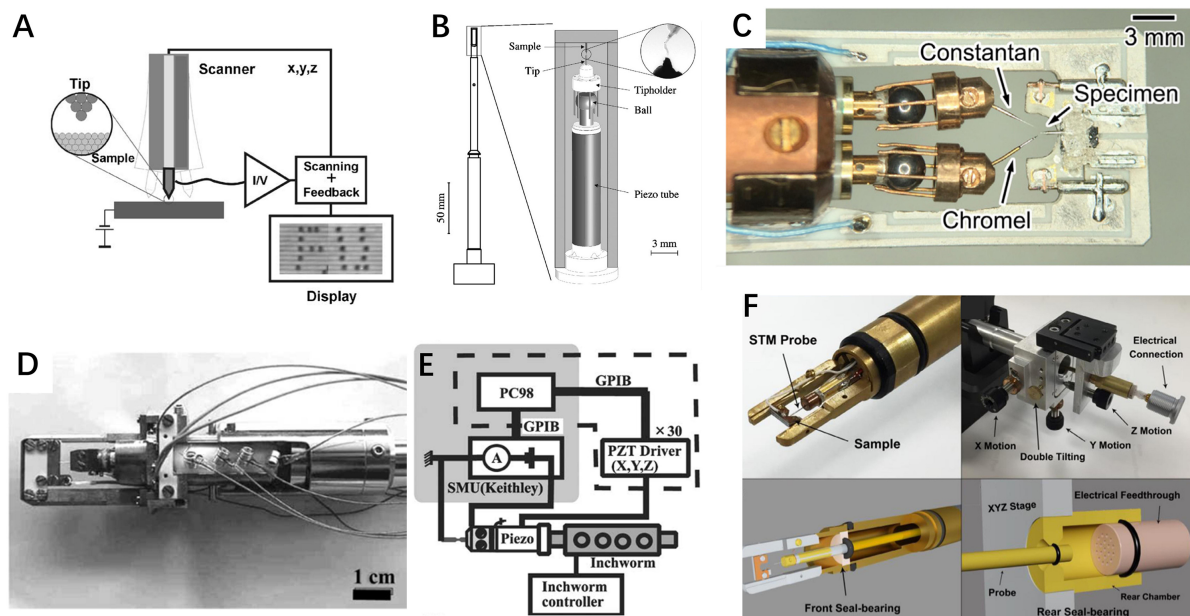


Figure 2. (A) The working principle of STM. Reproduced with permission^[55]. Copyright 2004, Elsevier. (B) Schematic illustration of the side-entry holder and its STM head with a three-dimensional coarse motion mechanism. The inset shows the *in-situ* selectively approaching process of a gold tip to a carbon nanotube with 20 nm in diameter. Reproduced with permission^[56]. Copyright 2003, AIP publications. (C) Top view of an optical image of a two-probe STM holder consisting of chromel and constantan piezo-driven probes and a thinned TEM specimen supported on a tungsten base. Reproduced with permission^[57]. Copyright 2018, Elsevier. (D and E) Photograph of the new STM holder designed for UHVTEM (JEM-2000VF) and the electronic circuit used for the conductance measurement. Reproduced with permission^[58]. Copyright 2003, Elsevier. (F) Photographs and schematics showing the design of the double-tilt *in-situ* TEM holder. Reproduced with permission^[60]. Copyright 2018, Elsevier.

sapphire ball fixed to a tube piezo, and the STM probe was connected to the sapphire ball by the springs. The probe can perform coarse motion in three dimensions, which is based on the stick-slip principle and is realized by applying sawtooth voltage pulses to the tube piezo^[56]. Based on such a holder, some other holders with diverse functions have been developed, as shown in Figure 2C, which has two STM probes for multifunctional applications^[57]. As shown in Figure 2D and E, Oshima *et al.* have designed a miniature STM system that was combined into TEM^[58] to achieve high-resolution images at ultra-high vacuum TEM (UHV-TEM, JEM-2000VF). A metal wire was placed in an intermediate position between the electrodes of the STM holder and then slowly stretched by a piezo actuator until the wire broke in the etched area and formed two metal electrodes. Electron beam irradiation was further employed to thin the suspended nanowires^[59]. Conductivity measurements were made by source measure unit, and synchronization between the TEM and conductivity measurements was achieved using a personal computer clock. Xu *et al.* have developed a seal-bearing double-tilt TEM-STM holder in which the coarse motion of the STM probe is controlled by a long rod and the fine motion is regulated by a piezoelectric tube piezo [Figure 2F]^[60].

Due to its simple structure, easy manipulation and sample preparation, TEM-STM is widely used to explore the mechanical properties of NMs. The development of multifunctional TEM-STM holders has also greatly extended their application possibilities. The biggest challenge of this method is that the force signal during deformation of a material cannot be measured using the current strategy. Therefore, it is difficult to conduct quantitative analysis on the mechanical properties of the NMs such as the Young's modulus and yielding point, *etc.*

TEM-AFM

AFM, which enables the detection of the force between the probe and the sample at the pico-Newton level, is one of the most important tools for characterizing the material properties. Depending on the mode of operation, it is usually classified into contact- and non-contact modes. The working principle of the contact mode AFM^[34] is to detect the force by measuring the deformation amount of a cantilever beam when the probe is attached to the free end. As shown in Figure 3A, the most common technique currently used to measure the amount of bending is the optical lever method. According to Hooke's law, the force magnitude acting between the probe and the sample is proportional to the deformation amount of the cantilever beam. The AFM microcantilever, which is made of single-crystal Si or Si₃N₄ and has a conical tip near its free end, is used for probing the sample surface through intermolecular forces. It can be used for lateral bending of the sample and determining the elasticity constants and thicknesses of thin films^[61]. When contact mode AFM is combined with TEM, the amount of deformation of the cantilever beam is usually determined from observations in the TEM, as shown in Figure 3B^[46]. Furthermore, some researchers have mounted a self-sensing cantilever AFM probe into a TEM holder, where the self-sensing of the AFM cantilever probe is realized by a Wheatstone bridge [Figure 3C]^[62].

In contrast to the contact mode described above, non-contact mode AFM, typically working with the probe separated from the sample, has also been used to investigate the mechanical properties of NMs. Different from the contact mode AFM that can directly measure the force, the non-contact mode AFM obtains the force gradient (so-called spring constant), which could be calculated from the shift of the resonant frequency of the sensor^[63]. Since the force response was obtained by modulating resonant frequency, non-contact mode AFM is also called frequency-modulated AFM (FM-AFM)^[63]. Four types of sensors are commonly used in FM-AFM: cantilever, tuning fork, Q-plus, and length extension resonator (LER)^[64]. The sensor works on the principle of the piezoelectric effect, where strain is generated when the sensor vibrates. The surface charge generated by the strain is collected by a metal electrode. The induced charge is converted into a voltage by a charge amplifier to provide information such as phase and amplitude to determine the resonant frequency of the sensor, as shown in Figure 3D. Based on a quartz tuning fork (QTF), the Q-plus sensor is a further development. As shown in Figure 3E, Q-plus is a quartz cantilever with a larger size than micromachined silicon cantilevers, which is suitable for mounting with various tips^[65]. Recently, an *in-situ* TEM holder using a quartz LER as a force sensor has been developed by Zhang *et al.* to study the size/crystal orientation-dependent mechanical properties of various NMs^[66]. The LER is a kind of non-contact mode AFM sensor with high stiffness, which can reduce the oscillation amplitude, enabling researchers to obtain atomic resolution TEM images during the force measurement. The used *in-situ* TEM holder is shown in Figure 3F. Employing it makes it possible to observe the atomic structure of NMs by TEM and precisely measure the mechanical response using force sensors simultaneously.

In summary, contact mode AFM can directly measure the applied force on nanocontacts, whereas the non-contact mode AFM provides the force gradient (spring constant). The choice of AFM modes depends on the measurement requirement and sample condition. For example, contact mode AFM is convenient for studying the plastic deformation properties and it is possible to measure the yield or fracture stress of the NMs by directly measuring the force. Conversely, non-contact mode AFM is more suitable for investigating the elastic properties due to the easy evaluation of elastic response from directly measured spring constant and elastic constant. To quantitatively analyze the elastic or plastic properties of the materials, the force signal should be combined with the captured structure evolution of the NMs. These structural evolutions are usually recorded in high-resolution videos and require frame by frame analysis, leading to a heavy work of data analysis.

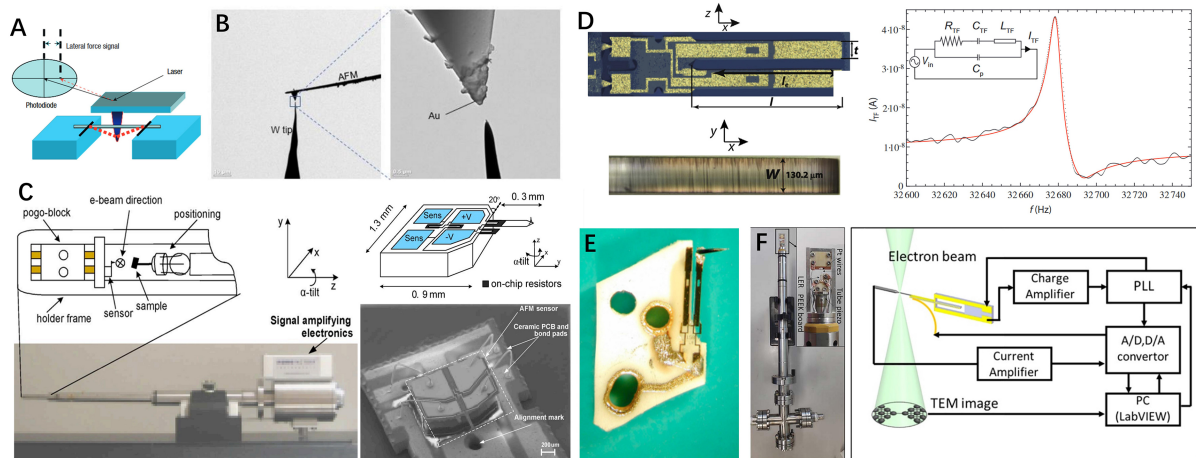


Figure 3. (A) Schematic of the lateral bending test of a fixed wire with an AFM tip. Reproduced with permission^[34]. Copyright 2005, Springer Nature. (B) Low magnification TEM images of the experimental setup. The spring constant of the AFM cantilever is 0.02 nN/nm. Reproduced with permission^[46]. Copyright 2021, Springer Nature. (C) The TEM holder with self-sensing AFM tips. Reproduced with permission^[62]. Copyright 2008, IEEE publications. (D) Left: Optical microscopy image of the used QTF. Right: Function between the driving frequency f and the amplitude of the current I_{TF} flowing through a QTF driven by a sinusoidal voltage with amplitude $V_{in} = 10$ mV. Inset shows the equivalent circuit diagram of a piezoelectrical resonator. Reproduced with permission^[52]. Copyright 2015, Elsevier. (E) Photograph of a Q-Plus sensor - a cantilever made from a QTF. Reproduced with permission^[65]. Copyright 2020, American Physical Society publications. (F) Photographs showing the self-developed TEM holder and an illustration of the measurement system. Inset shows the sample stage at the head of this holder. Reproduced with permission^[66]. Copyright 2020, IOP publications.

Strain device

Researchers have designed various devices in TEM holders for straining samples. Liu *et al.* designed a TEM tensile actuator to study the deformation process of NMs^[48]. The schematic in Figure 4A shows a pair of thermally actuated bimetallic arms attached to opposite locations on the TEM copper grid as a TEM tension actuator. Each arm comprises two layers of different materials, which have widely distinct thermal expansion coefficients, so that they can deflect considerably even at relatively low operating temperatures. The sample was first bridged between these two bimetallic arms, and then the TEM tension actuator was placed into a heating sample holder for observation. When the TEM tension actuator is heated, the different thermal expansion coefficients of the bimetals cause the arms to deform, thereby stretching the material. With this device, atomic resolution images can be obtained during the stretching of the sample, allowing the deformation mechanism of the material to be analyzed at the atomic scale^[67,68]. As shown in Figure 4B, Wang *et al.* developed an atomic-scale *in-situ* bending method for individual nanowires^[42]. We should notice that the condition of the sample is more complicated than the uniaxial loading, as it involved the coexistence of the zero strain, tensile strains and compressive strains within it. Considering such complex internal stress conditions, the analysis of elastic properties or deformation mechanisms should also be more cautious. Combining first-principles calculations and MD simulations may be an effective way for the data analysis. The nanowires were dispersed on a TEM grid covered by a pre-disrupted colloidal thin film. The dispersed nanowires are then controllably bent or stretched at low strain rates by the expansion or contraction of the colloidal thin film under the irradiation of the electron beam. With this method, the specimen can be tilted by a large angle in two orthogonal directions without the special mechanical tensile attachments. Thus, the deformation processes of bending or uniaxial stretching of a single nanowire can be recorded at the atomic scale. To study the mechanical properties of NMs, a strain device was used, which contains a copper straining grid and a silicon frame [Figure 4C]^[69]. The samples were fixed to the silicon frame glued to a copper grid. By stretching the copper grid, the silicon frame was deformed and the sample was stretched. *In-situ* TEM experiments realize the application of controlled displacements along the film and the measurement of dynamic response during stress relaxation. Strain was assessed by the measured

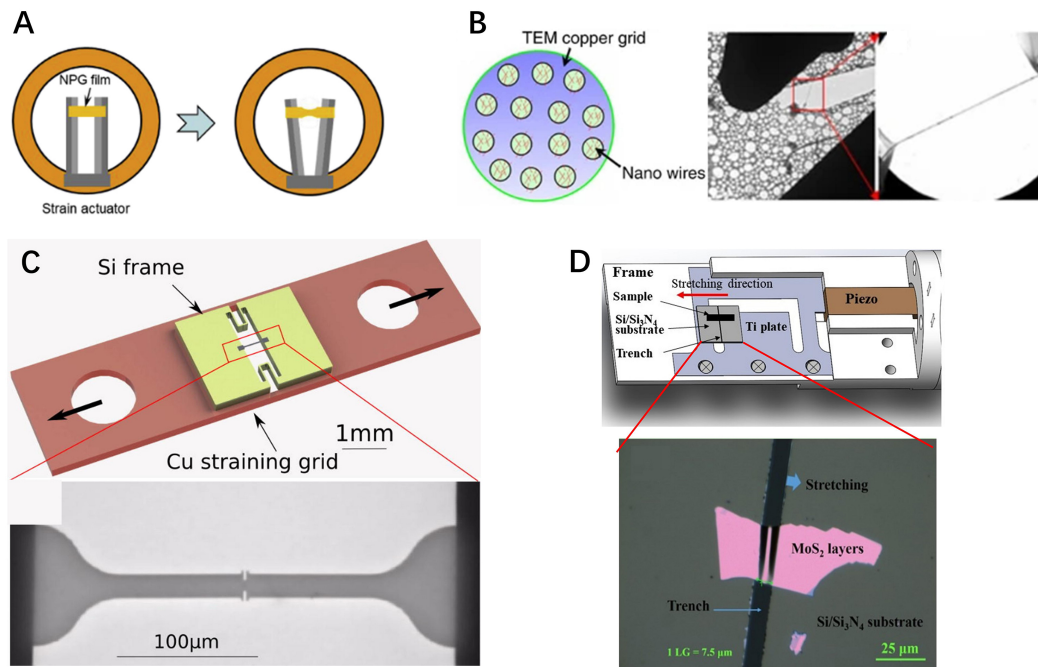


Figure 4. (A) Schematic of *in-situ* atomic-scale tensile testing of a nanoporous gold film using a home-built TEM strain actuator. Reproduced with permission^[48]. Copyright 2019, Elsevier. (B) Left side: A schematic view shows that the scattered Ni nanowires on a TEM grid covered by previously fractured colloidal thin film. Right side: Low magnification and enlarged (red framed region) TEM images show the deformation process of a single Ni nanowire by tensile stress induced by the under electron-beam irradiation. Reproduced with permission^[42]. Copyright 2013, Springer Nature. (C) Experimental setup with a TEM grid, where a dog-bone-shaped Al thin film was held on a MEMS. Reproduced with permission^[69]. Copyright 2015, Elsevier. (D) Diagram of the stretching TEM holder and the optical image of MoS₂ layers across the trench of the Si/Si₃N₄ substrate. Reproduced with permission^[70]. Copyright 2022, Elsevier.

change in gauge length of individual films. Xie *et al.* have developed an *in-situ* strain device to observe atomic resolution images of two-dimensional (2D) materials during their deformation, as shown in Figure 4D^[70]. Additionally, 2D material nanosheets are transferred and suspended between the gaps in the silicon chip, which is fixed to a specially shaped titanium plate. A piezo actuator is mounted on the end of the titanium plate. By applying a bias voltage to the piezo actuator, the piezo actuator pushes the titanium plate to deform, causing the gap of the silicon chip to become wider due to the deformation. As the width of the gap increases in proportion to the bias voltage applied to the piezo actuator, the 2D material will be stretched.

These strain devices usually have a simple construction, resulting in low maintenance costs and ease of use. These devices usually have very high stability to obtain atomic resolution TEM images due to the simple contractions. High-resolution TEM (HRTEM) images can also be acquired more easily by double-tilt sample holders. Similar to the TEM-STM method, the force signals are usually unavailable with these devices. Therefore, these devices can only attain dynamic processes during material deformation. In addition, the method tends to only stretch the material uniaxially and does not allow for compression, shear, or complex deformation.

TEM-MEMS

As micro-/nano-fabrication technology and MEMS/NEMS develop, researchers have designed and fabricated various mechanical test chips to measure the mechanical properties of NMs. Due to the small size

of the chip, it can be easily placed in a TEM sample holder to test the mechanical properties while performing TEM observation. The most common MEMS chip for mechanical measurement is a push-to-pull (PTP) device combined with TEM nanoindentation, which is used to stretch materials and study their mechanical properties. The SEM image in Figure 5A shows a typical PTP device consisting of a semicircular end and a specially designed cutout^[49]. The sample across the gap is subjected to uniaxial stretching by elongating the gap in the middle of the device when a diamond indenter pushes on the semicircular end. The nanoindentation device also simultaneously records the force and displacement of the nanoindentation punch. Its stiffness could be obtained by calculating the slope of the curve of the force applied to the PTP device versus the distance traveled by the nanoindentation indenter. The force-displacement curve of the sample is corrected after subtracting the force response of the devices. This *in-situ* tensile testing device can study the strain-induced microstructural evolution and mechanical properties of NMs.

Another TEM-MEMS device developed by Zhu *et al.* to study the mechanical properties of NMs, consisting of an actuator and a load sensor^[71], is shown in Figure 5B. The thermal actuators comprised of inclined beams can provide forces of up to tens of milli-Newtons and displacements of tens of micrometers. One end of the beam is connected to the shuttle and the other is fixed to the substrate. When applying a voltage to the inclined beam, the current induces Joule heating and thermal expansion, resulting in displacement of the actuator. The ensemble model of the load sensor is made up of two serially connected capacitors. The displacement of the shuttle causes capacitance change, thereby measuring the load applied to the material. Another mechanically tested MEMS device has been developed by Sato *et al.*^[72,73]. It consists of tips suspended by the soft springs and a two-degree-of-freedom electrostatic actuator that realizes longitudinal and lateral movements of the tip, as shown in Figure 5C. The movement of the tips was realized by adjusting the voltage applied on the electrode. Different from the above two MEMS devices, this device can apply not only axial but also shear loads. The shear force is calculated as the product of the arm stiffness and the displacement. Recently, Zhang *et al.* developed a state-of-the-art technique to realize *in-situ* deformation at temperatures up to 1,556 K with atomic resolution observation inside a TEM using a custom-designed device, as shown in Figure 5D^[74]. The TEM holder simultaneously tilts and deforms the sample at elevated temperatures while performing atomic resolution TEM imaging. Tensile samples are prepared by precisely transferring a block sample with a predetermined crystal orientation to the push-pull unit using a probe in the focused ion beam (FIB). The displacement of the sample is controlled with high accuracy by applying a voltage to the actuator during this process.

The structure of these MEMS chips is often exquisitely designed to enable mechanical testing. Combined with a double-tilt TEM sample holder, atomic resolution TEM images can be obtained very well^[73]. The force response and dynamic processes during sample deformation can be recorded simultaneously. In addition, multifunctional testing can be realized through more sophisticated designs, such as electrical, mechanical and thermal properties, *etc.* The sample preparation for this method is a little bit complicated and usually requires a FIB to cut the sample to a suitable size and shape, as well as fix it to the specified position for *in-situ* TEM observation. Some samples that are easily damaged by the ion beam are also difficult to measure through this method.

Nanoindentation & tensile gripper

Nanoindentation techniques and tensile fixtures are widely used in mechanical testing of bulk materials. In recent years, some researchers have miniaturized and integrated these devices into TEM sample holders to measure the mechanical properties of materials. Figure 6A shows a photograph of the common commercial Hysitron PI 95 TEM picoindenter and schematic illustration of the working mechanism^[50]. To perform a uniaxial compression test on a single nanowire using the holder, a substrate with vertically oriented

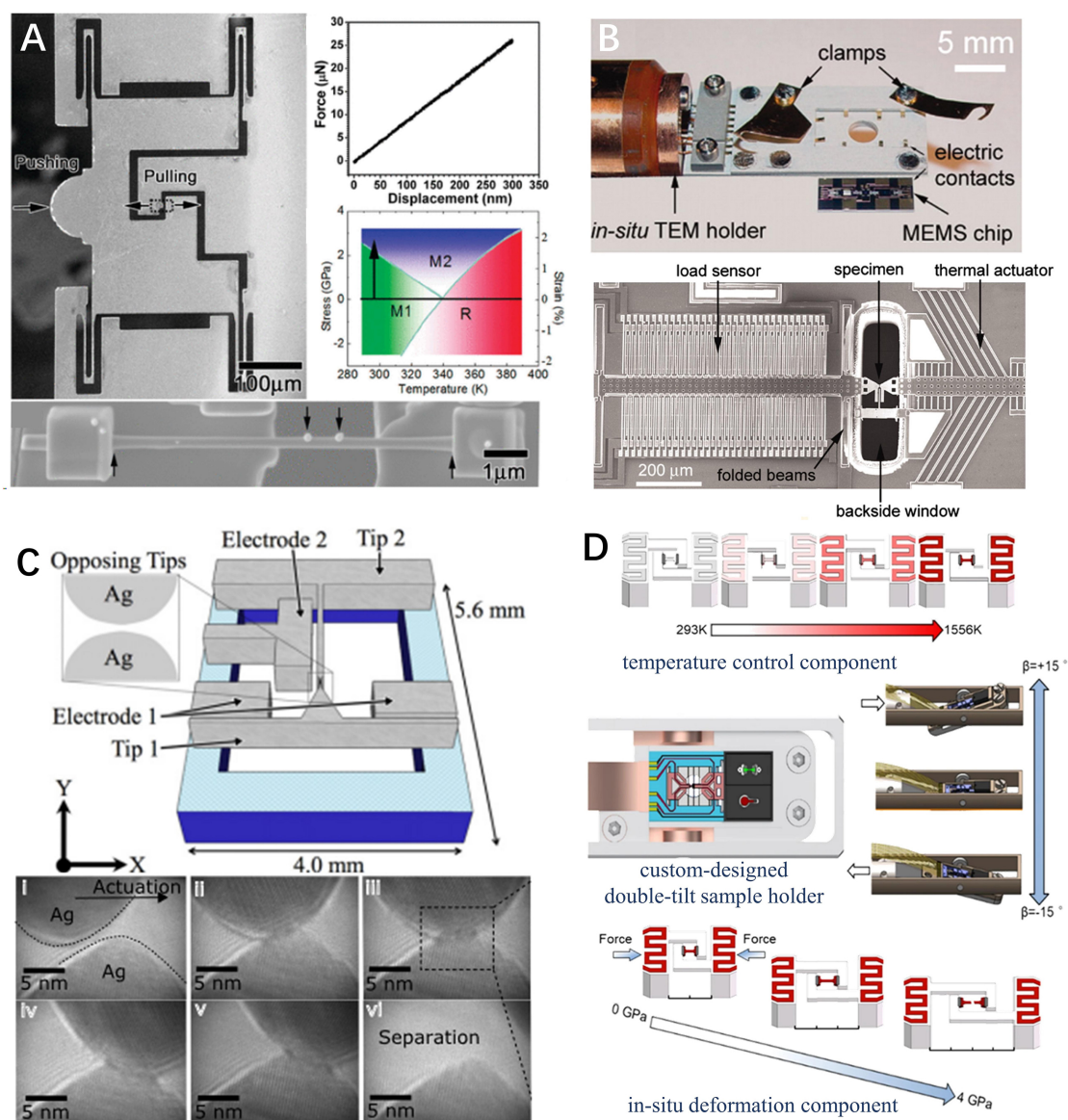


Figure 5. (A) SEM image of the microfabricated push-to-pull (PTP) chip and the corresponding force single measured by such chip. Reproduced with permission^[49]. Copyright 2011, ACS publications. (B) *In-situ* TEM holder (top) with a MEMS chip (bottom) for tensile testing. The MEMS chip consists of a load sensor, specimen and actuator, which was placed in a TEM holder in the experiment. Reproduced with permission^[71]. Copyright 2005, PANS publications. (C) Schematic of the silicon-based NEMS device and a series of TEM images of a single asperity sliding experiment. Reproduced with permission^[72,73]. Copyright 2022, Springer Nature. (D) A custom-designed double-tilt TEM holder with a high-temperature mechanical testing system, including the temperature control and the *in-situ* deformation components. Reproduced with permission^[74]. Copyright 2021, Springer Nature.

nanowires is carefully fixed to the holder so that the axial direction of the nanowires will be perpendicular to the diamond punch surface. A compressive load is then applied to the nanowire in a loading direction parallel to the nanowire axis, which is achieved by moving the punch toward the nanowires. The movement of the punch is controlled by a piezo. As the compressive load is gradually increased, the nanowire buckles before fracture. The force applied on the sample and punch movement are obtained simultaneously when the sample is deformed. In this case, the fracture strength and critical buckling load of nanowires would be easily determined from the stress-strain curve. As shown in Figure 6B, Nie *et al.* performed *in-situ* bending experiments using the XNano *in-situ* TEM sample holder^[44,75]. The sample was placed on a nano-

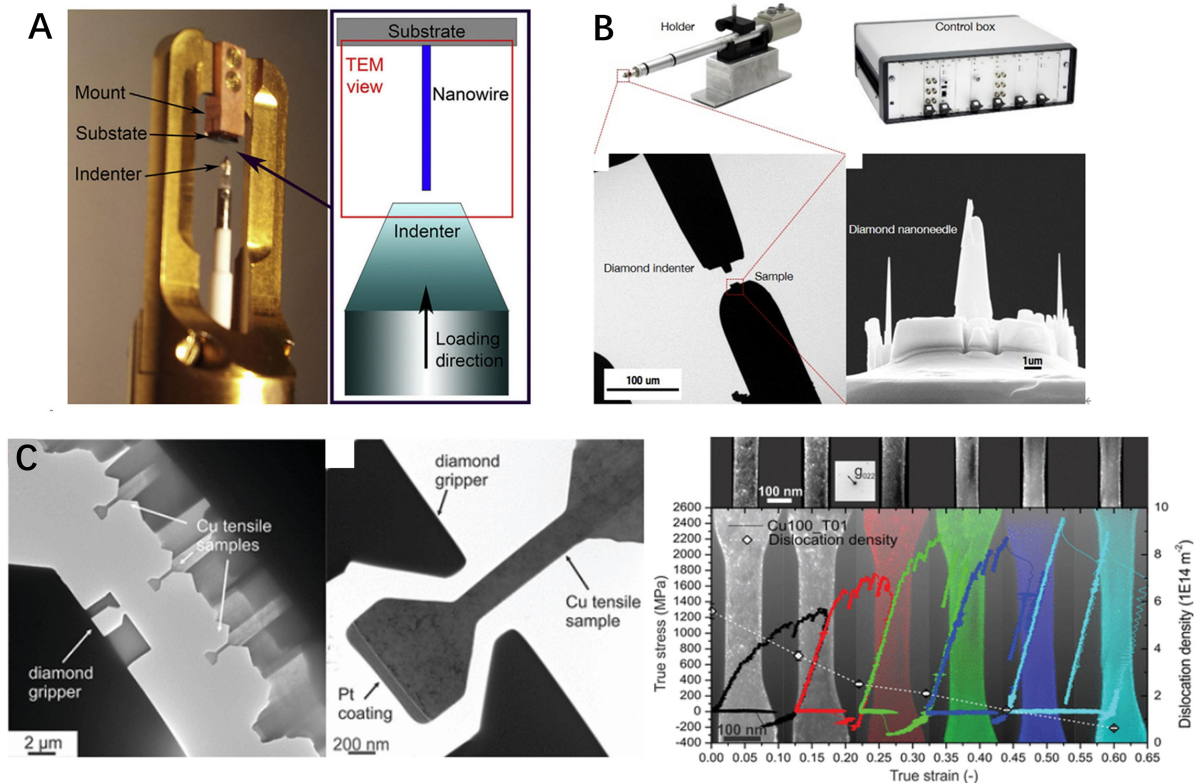


Figure 6. (A) Photograph and schematic illustration of the PI 95 picoindenter in TEM^[50]. Reproduced with permission. Copyright 2016, Elsevier. (B) The instrumentation and the experimental setup for the *in-situ* bending tests, including the XNano TEM holder and control box. Reproduced with permission^[44]. Copyright 2019, Springer Nature. (C) Left: The setup for *in-situ* TEM tensile tests with the structured conductive diamond tip acting as a gripper. Right: True stress versus true strain data for repeated loading of a tensile copper sample with an initial diameter of 133 nm and orientation of (100). Reproduced with permission^[45]. Copyright 2011, ACS publications.

manipulator with four degrees of freedom (three dimensions positioning plus self-rotation), and the motions are precisely controlled by the piezo actuators with an accuracy of about 0.1 nm. A diamond indenter was installed on the stage, and the samples were pushed against the indenter by the nano-manipulator.

Based on the nanoindentation device, materials can be sculpted into the shape of a "dog bone" for tensile testing using a FIB, as shown in Figure 6C. A gripper sculpted by FIB is fixed to the punch to clamp and stretch the sample. The excellent resolution of TEM provides enables highly accurate alignment of in-plane orientations. After aligning the height of the tensile specimen to the top of the gripper by means of the focus of TEM, the specimen is then lowered to the middle of the gripper using the piezo actuator. The gripper is then moved backward to stretch the specimen. These methods are usually used to measure samples in large sizes (several hundred nanometers). However, the large sample size may cause significant drift during the stretching process, making it difficult to obtain atomic resolution images during the tensile process.

MECHANICAL PROPERTIES OF NANOMATERIALS

Elastic properties

Young's modulus is defined as the ratio of uniaxial stress to the amount of deformation within the range of application of Hooke's law. The stiffness of a material is indicated by the magnitude of its Young's modulus; the greater the Young's modulus, the less likely the material is to deform. Young's modulus is a commonly

used parameter in engineering and technical design, and its accurate determination is very important for studying the mechanical properties of various materials such as metals/semiconductors, optical materials, NMs, polymers, ceramics, rubbers, *etc.* It can also be used in designing mechanical components, biomechanics, geology, and other fields^[76]. For atomic-scale materials, the magnitude of Young's modulus reflects the strength of interatomic forces between neighboring atoms or ions, which vary depending on the type of bonding in the material. For bulk materials, it is an intrinsic property and is independent of the material size. In contrast, for nanoscale materials, theoretical studies have shown that it is related to the material size due to the surface effect^[77,78]. The *in-situ* TEM technique is regarded as a powerful tool for measuring the Young's modulus of a material because the dimensions, atomic-scale structures and deformation could be obtained by TEM. By combining high-precision mechanical sensors, the elastic properties of samples with a specific structure can be accurately obtained. The influence mechanism of Young's modulus can also be analyzed at the atomic scale.

When materials are scaled down to the nanoscale, their Young's modulus is also different from that of the bulk material due to the surface effect, quantum confinement effect, and so on. The Young's modulus of a material is usually associated with its size. However, researchers are still exploring whether smaller is stiffer or smaller is weaker. As shown in Figure 7A, Dai *et al.* characterized the Young's modulus of gallium nitride (GaN) nanowires with different structures using *in-situ* electron microscopy^[79]. Using the electric field-induced resonance method, it was found that the Young's modulus of single-crystal GaN nanowires along the [120] direction was similar to the bulk value for diameters of 92–110 nm, and there was no size-dependent Young's modulus for diameters of 98–171 nm. Chen *et al.* investigated the elasticity of defect-free single crystal and high density stacking fault (SF) gallium arsenide (GaAs) nanowires using *in-situ* TEM compression combined with finite element analysis [Figure 7B]^[80]. They found that the presence of a high density of SFs increased the modulus of elasticity by 13% and that the Young's modulus of the same structured nanowires increased with diameter reduction which indicates “smaller is stiffer”. Wang *et al.* reported that size has a significant effect on the mechanical properties of GaAs nanowires, with the Young's modulus of the nanowires increasing with decreasing size, as shown in Figure 8A. Nanowires with diameters of 50–150 nm have an elastic strain of 11%, and those with diameters ≤ 25 nm have significant plastic deformation. The Young's modulus of GaAs nanowires is more than twice that of the bulk^[81]. Liu *et al.* find that the Young's modulus of molybdenum disulfide (MoS₂) nanoribbons also increase as the size declines^[82].

For the metal case, it is reported that the Young's modulus of Au nanowires shows size independence with diameter in the range of 50–200 nm^[34], whereas the yield strength rises with diminishing nanowire diameter. As the nanocontact diameter decreases below 2 nm, the Young's modulus progressively decreases from 80 to 30 GPa due to surface softening. Furthermore, the monoatomic chains and bonding stiffness can also be achieved using *in-situ* TEM. As shown in Figure 8B, Zhang *et al.* use a LER as the force sensor to measure the elastic properties of Au nanocontacts. They found that the Young's modulus of Au nanocontacts reduced with decreasing diameter, showing that “smaller is softer”^[22]. They propose that the surface atoms have a low Young's modulus, while the core atoms have a Young's modulus similar to the bulk one.

Despite no consensus on the relationship between size and Young's modulus, more experimental results indicate that smaller covalently bonded materials are stiffer, and smaller metallic materials are softer. Previous theoretical studies have pointed out that the size effect of Young's modulus is determined by the competition between the weakening caused by the lower coordination number of surface atoms and the hardening caused by the redistribution of surface electrons. Thus, different chemical bonds can lead to distinct size effects^[23,29,83,84].

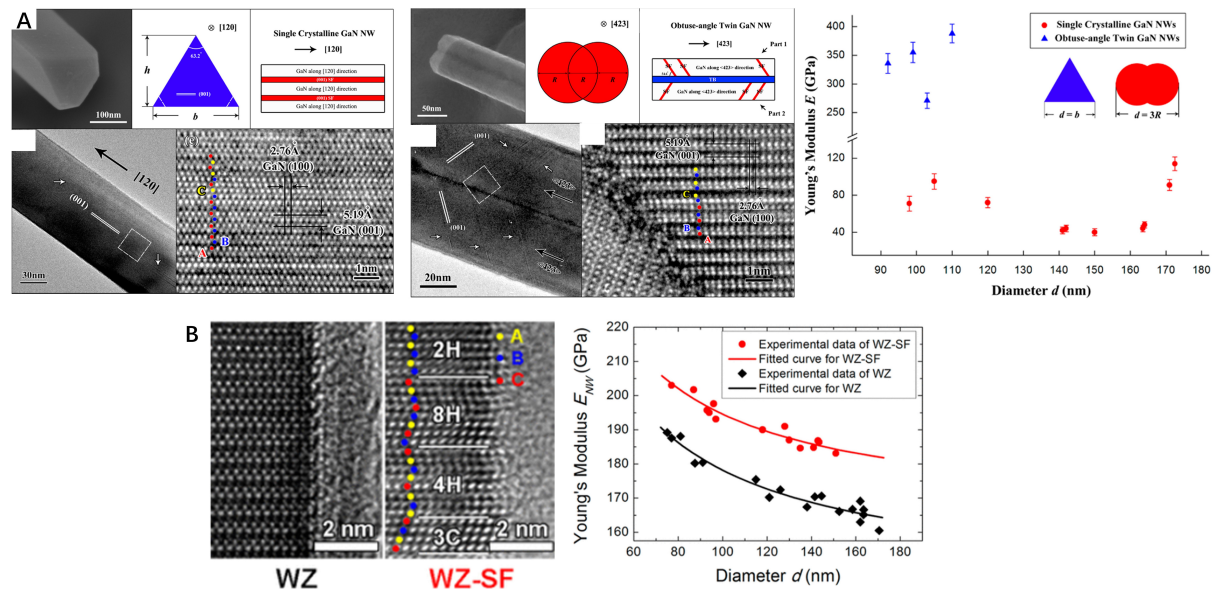


Figure 7. (A) Typical characterization results of single crystalline GaN nanowires and measured Young's modulus E versus characteristic diameter d of total 14 GaN nanowires. Reproduced with permission^[79]. Copyright 2014, ACS publications. (B) Left: High-resolution TEM (HRTEM) images of GaAs nanowires with hexagonal wurtzite (WZ) and WZ with a high density of stacking faults (WZ-SF) structure, respectively. Right: Measured corresponding effective Young's modulus of WZ (black diamond) and WZ-SF (red circle). Reproduced with permission^[80]. Copyright 2016, ACS publications.

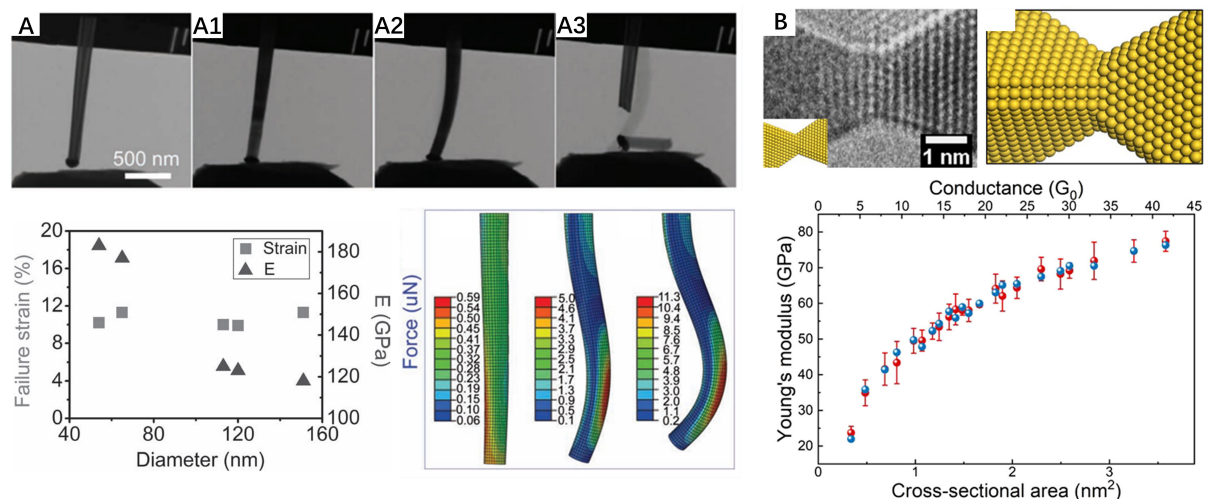


Figure 8. (A) Top: Sequential TEM images of a GaAs nanowire during *in-situ* compression tests. Bottom: Relationships between failure strain, Young's modulus and mean diameter of GaAs nanowires obtained from finite element analysis (FEA) results based on experimental data and FEA models corresponding to the states in TEM images (A1-A3), respectively. Reproduced with permission^[81]. Copyright 2011, Wiley-VCH GmbH. (B) The TEM image and size-dependent Young's modulus of the Au nanocontacts. Reproduced with permission^[22]. Copyright 2022, American Physical Society publications.

In addition to the Young's modulus, elastic strain is another important parameter of elastic properties of a material, defining the maximum strain that a material can withstand before it undergoes plastic deformation or brittle fracture. NMs tend to exhibit elastic strains close to the theoretical limit due to their smaller size and, therefore, fewer defects. Through *in-situ* TEM technology, Nie *et al.* found that the diamond nanoneedle had a huge reversible elastic deformation, which depended on the diameter and

orientation of the nanoneedle [Figure 9A]^[44]. The highest elastic tensile strain (13.4%) and tensile strength (125 GPa) were successfully measured from a 60 nm diameter $\langle 100 \rangle$ oriented nanoneedle. By cutting diamond into nanorods with FIB, Dang *et al.* found that the elastic strain of nanodiamond reached 9.7%. They predict that the transition of indirect-direct bandgap may occur when the tensile strain is larger than 9% [Figure 9B]^[47]. Zhang *et al.* found that the elastic strain of ~100 nm diameter single-crystal Si nanowires could reach 16% at room temperature, which is close to the theoretical elastic limit of silicon (17% to 20%). The fracture stresses were estimated up to about 20 GPa [Figure 9C]^[43]. Zhang *et al.* found that the bond stiffness between the two atoms in the middle of one-dimensional Pt monoatomic chains was measured to be about 25 N/m and the maximum elastic strain of a single Pt-Pt bond was about 24%^[85].

Plastic properties

The plasticity of bulk materials is usually related to dislocations and the interaction between dislocations and grain boundaries (GBs). Numerous experimental results show that the deformation mechanism of NMs is much different from that of their bulk counterparts.

For example, dislocation density in coarse-grained metals will increase with plastic deformation due to the dislocation accumulation, whereas for nano metallic materials, dislocation starvation caused by deformation has been predicted and observed because dislocations will disappear at the free surface. As shown in Figure 10A, Sun *et al.* found that silver (Ag) nanowires with a diameter of 5 nm were plastically deformed under tension through partial dislocation activity, leading to twinning and uniform elongation of the nanowires, while surface atomic diffusion reduced the width of the nanowires^[52]. Finally, the axial direction of the nanowires ultimately changes from its original $\langle 112 \rangle$ to $\langle 110 \rangle$. In addition, Li *et al.* discovered that the deformation modes of nanosized metals can be predicted from the ratio of the energy barriers of the FCC to the hexagonal close-packed (HCP) phase transition ($\Delta\gamma_H$) and the deformation twin nucleation ($\Delta\gamma_T$), which differ from those of the theoretical modes of relatively large-sized metals^[86]. Surface atomic diffusion begins with a surface step introduced by partial dislocation activity, leading to nanowire fracture. Plastic deformation dominated by incomplete dislocations is also observed in palladium (Pd) nanowires. The deformation behavior of NMs of different sizes also varies; for example, Si nanowires with diameters of 310-400 nm show a brittle to ductile transition in the compression experiment^[87]. Wang *et al.* found that due to dislocation nucleation, movement, and interaction and amorphization, Si nanowires with diameters of 60-100 nm exhibit large plastic strains at room temperature^[88]. Recently, researchers have found that the thickness and strain are the key factors that can effectively modulate the phases of 2D In_2Se_3 . The reversible antiferroelectric and out-of-plane ferroelectric phase transitions in 2D In_2Se_3 were controlled by the strain control inside a TEM^[89].

For single-crystal Au nanowires, Liu *et al.* used an aberration-corrected TEM to observe the deformation process of nanoporous gold and proposed an atomic mechanism for nanopore-induced embrittlement of ductile metals^[48], as shown in Figure 10B. They found that the brittle deformation of the nanoporous gold arises from the interplay of the dislocation plasticity and the stress-driven surface diffusion. Seo *et al.* reported the coherent twin propagation induced superplastic deformation of Au nanowires^[90]. The initial $[110]$ oriented nanowire was converted to a $[100]$ oriented one. Chu *et al.* combined *in-situ* TEM and Monte Carlo simulations and found that in nanocrystals, edge dislocation climbing occurs by stress-induced reconfiguration of two adjacent atomic columns at the edges of an additional half-atomic plane in the dislocation core [Figure 10C]^[91]. This differs from the conventional view that dislocation climbing occurs by destruction or reconstitution of individual atomic columns in the dislocation core. In addition to observing the plastic behavior of NMs by various *in-situ* techniques, as shown in Figure 10D, Wang *et al.* demonstrated that Au nanowires containing twin crystals with a thickness of 0.7 nm had tensile strengths of up to 3.12 GPa, which is close to the ideal limit, and showed a significant toughness-brittleness transition

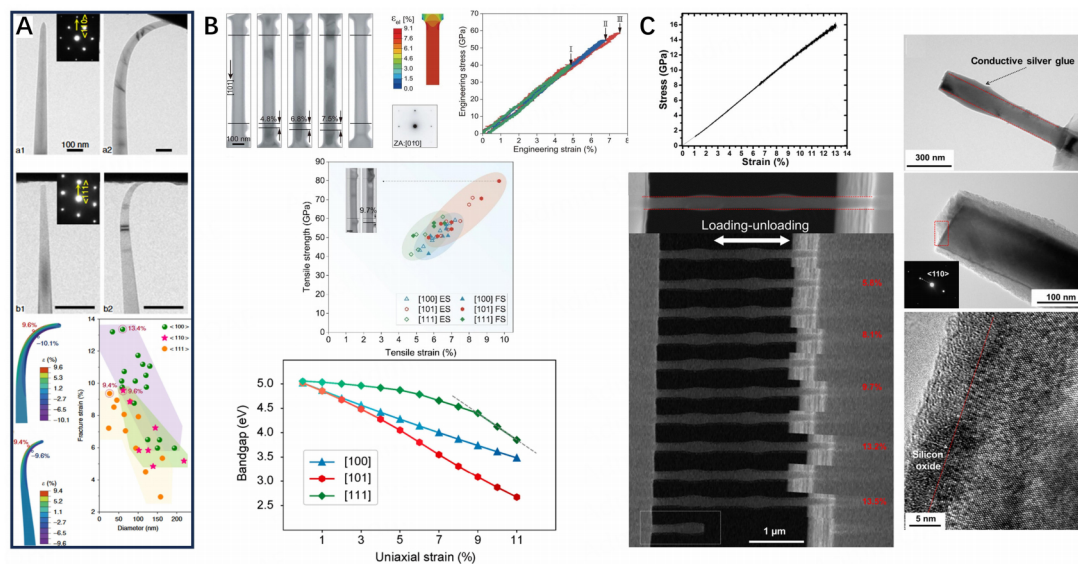


Figure 9. (A) Orientation and size-dependent fracture of diamond nanoneedles. Reproduced with permission^[44]. Copyright 2019, Springer Nature. (B) Top: Elastic loading-unloading deformation process of the diamond along the [101] direction and the corresponding FEM simulations. Middle: The statistical tensile results of diamonds oriented along [100], [101] and [111] directions. Bottom: The relationship of uniaxial strain and calculated bandgap values along [111] direction shows that indirect-to-direct bandgap transition occurs around ~9% tensile strain. Reproduced with permission^[47]. Copyright 2020, The American Association for the Advancement of Science. (C) *In-situ* SEM tensile tests and postmortem TEM analysis of a single Si nanowire. Reproduced with permission^[43]. Copyright 2016, Science Advances.

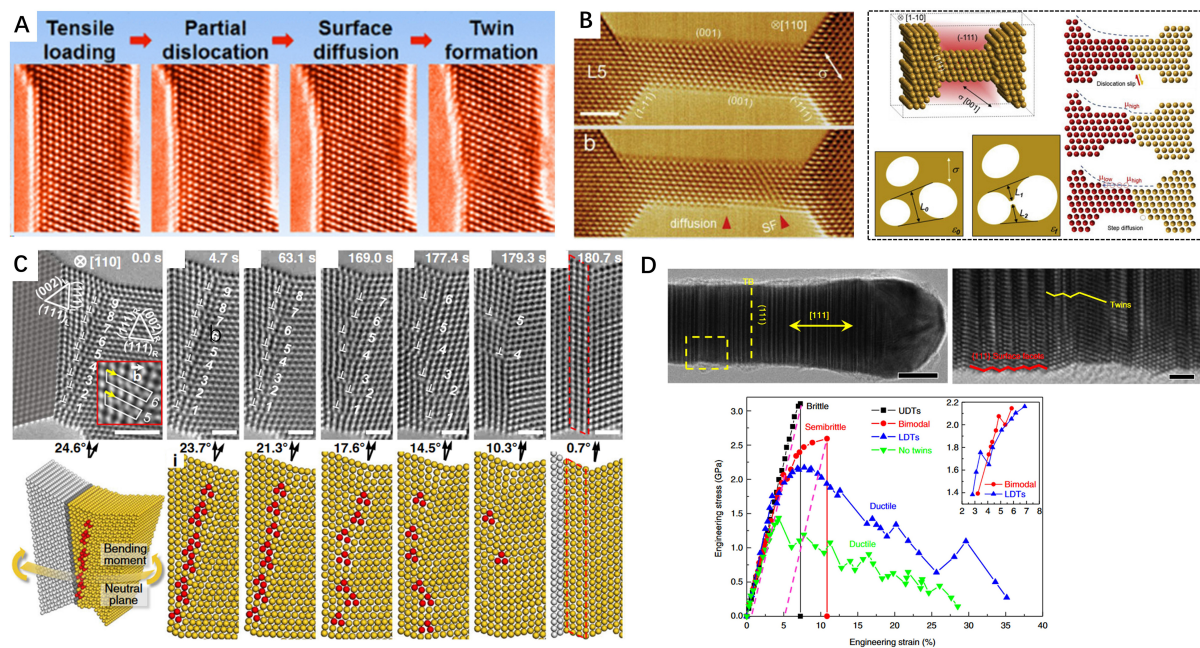


Figure 10. (A) Sequential *in-situ* HRTEM images during the tensile deformation process of an Ag nanowire. Reproduced with permission^[52]. Copyright 2019, ACS publications. (B) Left: Slip-activated surface diffusion occurring with the formation of stacking faults in nanoporous gold. Right: Schematic illustration of the thinning process of gold nanowire, which is through the slip and slip-activated surface diffusion. Reproduced with permission^[48]. Copyright 2019, Elsevier. (C) *In-situ* HRTEM images of dislocation climb at a high-angle grain boundary at room temperature and the corresponding reconstructed atomic models. Reproduced with permission^[91]. Copyright 2022, Springer Nature. (D) TEM images and stress-strain curves of ultra-twinned Au nanowires from *in-situ* TEM-AFM experiments. Reproduced with permission^[92]. Copyright 2013, Springer Nature.

with decreasing twin size^[92]. They propose that ultra-high density twins cause homogeneous dislocation nucleation and plastic shear localization, in contrast to the heterogeneous slip mechanisms observed in single crystals or low density twinned nanowires. Zhu *et al.* proposed that custom-designed low-angle GBs with controllable misorientation can be endowed with long-lasting cyclic deformability of metal biocrystals via GB migration to achieve controllable plasticity reversibility of metal nanocrystals^[93]. This reversible deformation is preserved in a large class of low stacking energy FCC metals when the GB structure, external geometry and loading conditions are extensively tuned. Both *in-situ* nanomechanical testing and atomistic simulation have demonstrated that the custom-designed low angle GB has controllable misorientation. This completely reversible plasticity is mainly controlled by the conservative motion of Schockley partial dislocation pairs, fundamentally suppressing damage accumulation and maintaining structural stability. The alloys feature different mechanical properties compared to the pure metals, mainly due to the chemical composition inhomogeneity. For example, Yang *et al.* found that AuCu alloy nanowires exhibit ~260% ultra-high plasticity and ~6 GPa ultra-high strength, which is due to the generation of HCP phase, reversible FCC-HCP phase transition, and zigzag-like nanotwins^[94]. Fu *et al.* found the AuAg alloy has three types of detwinning mechanisms, which is different with pure metals^[95].

For NMs, the role of surface atoms and defects such as dislocations on plastic deformation becomes more pronounced. With the atomic-scale resolution of TEM and advanced *in-situ* mechanical testing technology, the effect of these defects and surfaces on plastic deformation can be well studied. In the future, studying the effect of atomic-scale structure on the mechanical elasticity of NMs will remain an issue of great interest to scientists.

Viscoelastic properties

Viscoelasticity is one of the important mechanical properties of materials that dissipate energy during deformation. Although both plastic and viscoelastic deformation can be used for molding and result in energy dissipation, they are significantly different when unloaded to zero stress. A plastic part will always maintain its deformed shape because it has no fixed shape memory, whereas a viscoelastic part will always return to a certain shape regardless of its previous deformation history. In single-crystal materials, viscoelastic behavior is usually very small or negligible at the macroscopic scale. However, it becomes more significant when the size is at the nanometer scale. For example, Cheng *et al.* observed viscoelasticity in single-crystal ZnO nanowires and P-doped Si that is four orders of magnitude greater than the maximum viscoelasticity in bulk materials [Figure 11A]^[54]. As shown in Figure 11B, Chen *et al.* observed the viscoelasticity of small-diameter GaAs nanowires^[96]. Further studies revealed that the observed viscoelasticity was sensitive to the diameter of the nanowires and was significantly affected by the amorphous/crystalline interface on the nanowire surface. In addition, viscoelastic behavior is also observed in twinned copper oxide (CuO) nanowires of 17 nm, which may be related to the movement of atoms near the twin boundary^[97].

Viscoelasticity at the nanoscale is usually associated with the migration and recovery of defects. Through *in-situ* TEM techniques, Sun *et al.* have observed the viscoelastic deformation of sub-10 nm Ag nanowires, as shown in Figure 12A^[98]. By compression, the Ag nanocontact undergoes drastic deformation during which their external morphology undergoes a droplet-like change. Then, it surprisingly begins to regain its original shape by stretching and the basal diameter decreases from 14.3 to 9.5 nm in the first stage and then decreases to 9.2 nm, indicating a viscoelastic deformation process. Surface diffusion, rather than the dislocation slip normally expected at room temperature, is the atomic mechanism behind this shape evolution. For body-centered cubic (BCC) tungsten nanocrystals, Wang *et al.* demonstrated that twinning is the main deformation mechanism using *in-situ* HRTEM and atomistic simulations, as shown in Figure 12B^[99]. Such deformation twins are viscoelastic and exhibit reversible deconvolution during

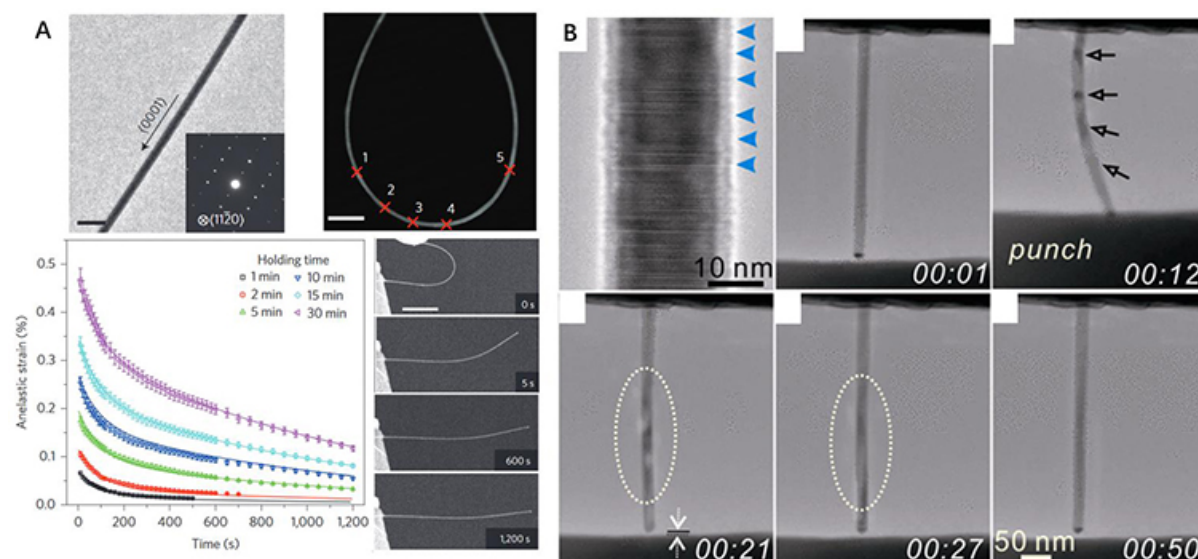


Figure 11. (A) *In-situ* SEM bending test and time evolution for anelastic of ZnO nanowires. Reproduced with permission^[54]. Copyright 2015, Springer Nature. (B) TEM micrographs showing the mechanical response of a GaAs nanowire with a high density of stacking faults. Reproduced with permission^[96]. Copyright 2013, ACS publications.

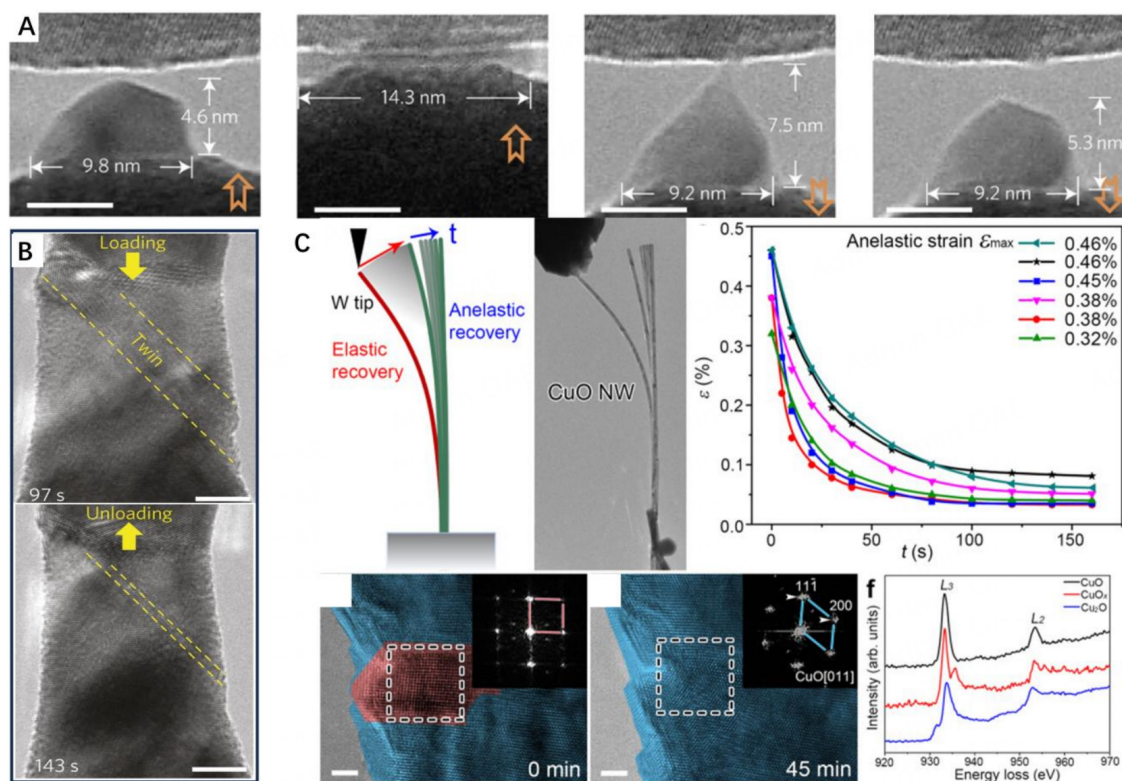


Figure 12. (A) TEM images showing the liquid-like behavior of sub 10 nm Ag nanoparticles. Reproduced with permission^[98]. Copyright 2014, Springer Nature. (B) Reversible deformation twinning and detwinning processes in a tungsten bicrystal nanowire under cyclic loading. Reproduced with permission^[99]. Copyright 2015, Springer Nature. (C) Anelasticity in single crystalline CuO nanowires. Reproduced with permission^[100]. Copyright 2021, Springer Nature.

unloading. In nanoscale BCC crystals, twinning and dislocation slip competition can be modulated by the orientation of the load, which could be attributed to the competitive nucleation mechanism of defects. Li *et al.* found that the stress-induced reversible migration of oxygen vacancies results in unexpected viscoelastic deformation of CuO nanowires at room temperature [Figure 12C]^[100]. The viscoelastic strain is related to the nucleation of the oxygen-deficient CuO_x phase, and after the stress is released, a gradual recovery of the nanowire shape is observed with the transformations from CuO_x back to CuO. The viscoelasticity found in NMs opens up the prospect of using NMs in nanoscale damping systems such as advanced micro/nanodevices.

For the viscoelasticity of materials, the *in-situ* TEM technique not only records important information such as the amount of deformation and the recovery time of the material but also analyzes the structure and compositional distribution of the material through atomic resolution images and spectrum. Thus, the fundamental mechanism of the emergence of viscoelastic behavior of nanoscale materials can be revealed.

Fracture

Fracture behavior is an important research area that is of great significance to understanding the strength and stability of materials, and it can provide an important reference for the design and engineering application of materials. Studying fracture behavior involves the fracture mechanics of materials, the causes and mechanisms of fracture, and the morphology of the fracture surface after fracture. Investigating fracture behavior and its mechanism is important for applying NMs in nanoscale electromechanical devices. During the measurement, a force sensor was used to measure the force applied to the sample and the fracture strength. Lu *et al.* investigated the mechanical behavior of Au nanowires below 20 nm under uniaxial tensile loading by HRTEM^[51]. There are two modes of fracture, including ductile fracture and the unexpected brittle fracture in the single-crystalline sub-20 nm ultrathin Au nanowires, whose fracture behavior is closely related to the observed twin-crystal structure and surface dislocation nucleation and propagation [Figure 13A]. They also found that sub-10nm <111> Au nanowires have ultra-high yield and fracture strengths (~7 GPa) that are close to the theoretical limits (~8 GPa), which may be caused by the surface dislocation nucleation. The fracture strength of amorphous carbon was measured to be ~15 GPa at the corresponding tensile strain of ~10% under the homogeneous plastic deformation. These values are close to the theoretical ones.

Beyond fracture strength, *in-situ* TEM can also observe the fracture surfaces of NMs at the sub-nanometer resolution, thus providing atomic-scale information for analyzing the fracture mechanisms of materials. Due to the smaller size of the NMs, many peculiar fracture phenomena have been observed. For example, the atomic-scale fracture process of 2D rhenium disulfide (ReS₂), MoS₂ and graphene was obtained using *in-situ* aberration-corrected scanning TEM (STEM). The brittle fracture of 2D ReS₂ with non-blunted crack tips and the perfect healing of cracks was observed^[101]. It has been reported that the fracture mechanism of MoS₂ can be changed from brittle to ductile by migration of S vacancies in the strain fields into networks as the defect density is increased^[102]. In addition, the fracture toughness and failure of 2D materials such as MoS₂ and graphene have also been reported to be related to the introduction of random distribution of atomic-scale defects^[103,104]. As shown in Figure 13B, Qiu *et al.* found that the fractured nanodiamond composites exhibited self-healing behavior at room temperature^[105]. Quantitative analysis showed that the self-healing characteristics of the composites originated both from the formation of nanoscale diamond osteoblasts consisting of sp² and sp³ hybridized carbon atoms on the fracture surfaces. Such self-healing behavior also results from the change of atomic interactions from repulsion to attraction when two fracture surfaces were getting close to each other. The self-healing process resulted in a significant recovery of ~34% in its tensile strength. Furthermore, the extraordinarily large viscoelasticity of the fracture surfaces of the nanogold crystals was also revealed by *in-situ* TEM experiments, as shown in Figure 13C. The liquid-drop-like viscoelastic strain varied from 31.4% to 81% after fracture^[21].

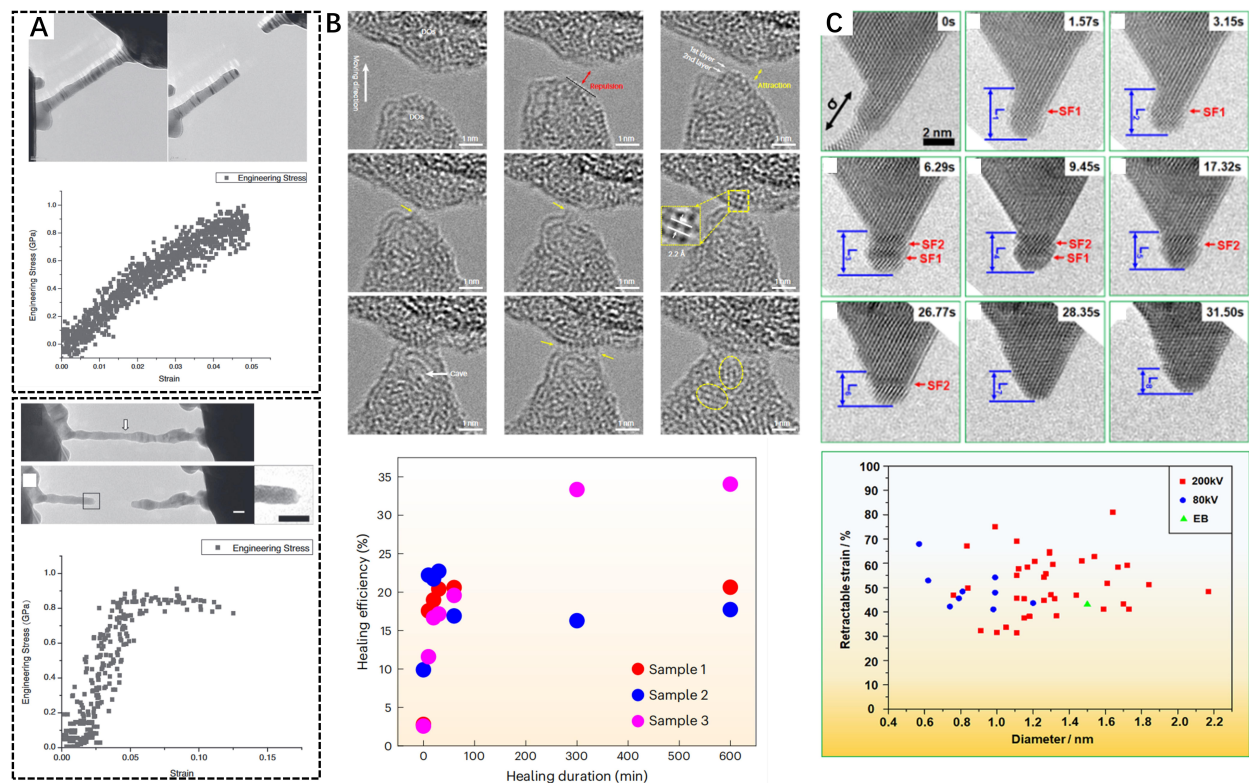


Figure 13. (A) Typical brittle fracture (top) and ductile fracture (bottom) of long gold nanowires during *In-situ* tensile tests. Reproduced with permission^[51]. Copyright 2011, Wiley-VCH GmbH. (B) Top: *In-situ* TEM observation of two fracture surfaces with diamond osteoblast protrusions during healing process. Bottom: The healing efficiency versus multiple fracture and healing durations of three ~200 nm wide nanotwinned diamond composite nanobeam samples. Reproduced with permission^[105]. Copyright 2023, Springer Nature. (C) Top: Typical example of a fractured gold nanowire with a retractable strain of 46.9%. Bottom: Statistical results of the retractable strain of gold nanowires with different diameters. Reproduced with permission^[21]. Copyright 2019, ACS publications.

In summary, NMs tend to exhibit peculiar fracture behavior due to their smaller size and larger specific surface area. The *in-situ* TEM technique with mechanical sensors allows not only quantitative measurements of fracture strength but also atomic-scale analysis of fracture surfaces. It has an irreplaceable position in the study of fracture behavior of NMs.

Friction

Friction is detrimental to the functioning of mechanical components of a product and is a major cause of equipment failure and unintended energy dissipation^[106-109]. Many nanoscale friction phenomena, such as in ceramics, metals and 2D materials, have been identified using AFM-based techniques^[110-113]. However, much of the current understanding of the friction phenomena lacks direct observation of the atomic-scale structure of the friction surfaces, and thus the relationship between the interface structure and friction mechanism has not been fully elucidated. *In-situ* TEM techniques, which enable us to measure the friction force while observing the friction behavior, are a powerful solution for these problems. Taking metal materials as an example, Wang *et al.* observed the friction process of tungsten single-asperity by HRTEM, as shown in Figure 14A. They found that the top layer of tungsten asperity showed a stick-slip motion behavior, and the evolution of the strain energy was explored by MD simulations^[53]. During friction, there is an asynchronous accumulation and release of strain energy at the friction interface and a non-uniform motion of the interfacial atoms. The contact area may play a more important role in atomic friction than the

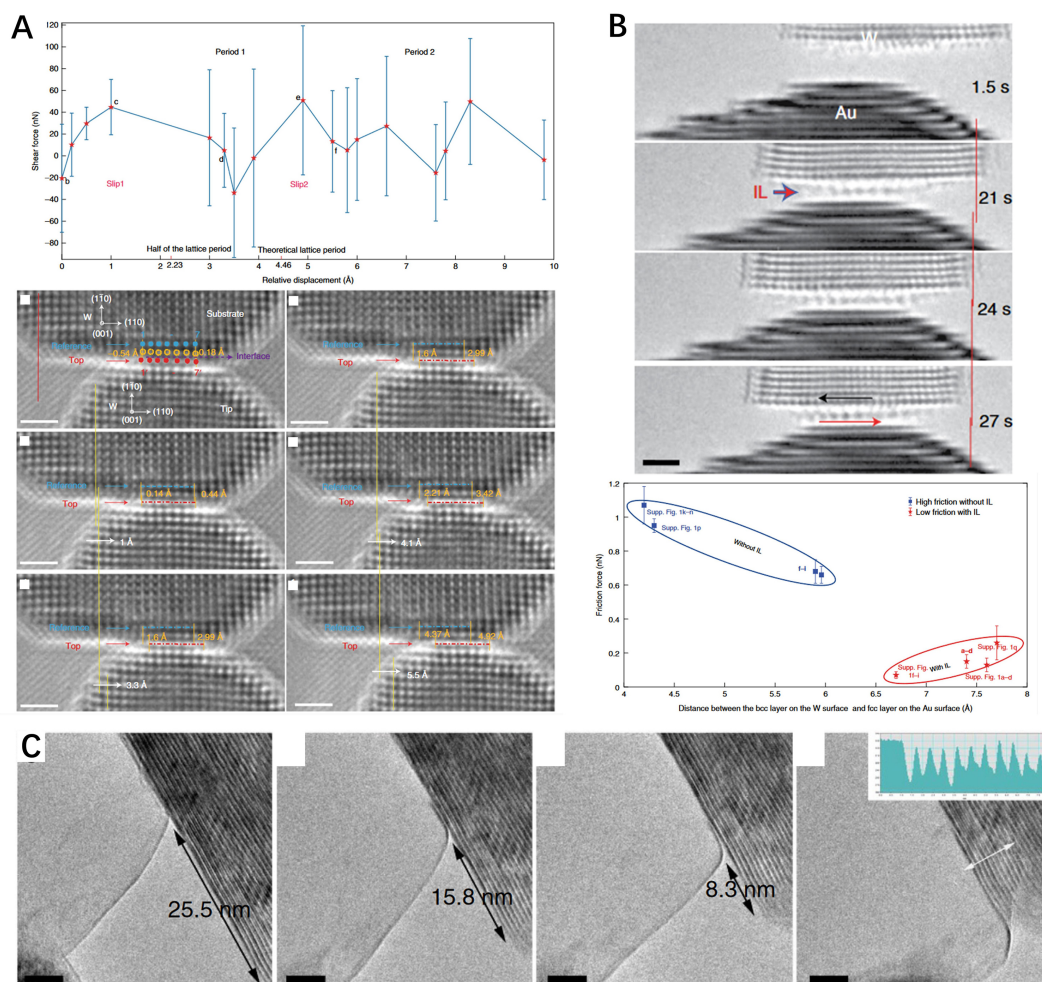


Figure 14. (A) *In-situ* TEM observation of stick-slip behavior between single tungsten asperity nanocontacts at the atomic scale. Reproduced with permission^[53]. Copyright 2022, Springer Nature. (B) A series of HRTEM images of a loosely packed interfacial layer (IL) induced low friction process between upper tungsten and lower gold asperities under tensile stress and statistics of the friction behaviors with and without an IL. Reproduced with permission^[46]. Copyright 2021, Springer Nature. (C) Sequential TEM images showing the high reversibility of cleaved monolayer MoS₂, which could be readily restacked onto the surface of the 'mother' crystal. Reproduced with permission^[116]. Copyright 2014, Springer Nature.

normal load. He *et al.* found that a loose interfacial layer was formed between two metal tips [Figure 14B]. The loose interfacial layer was formed by atomic diffusion under tensile stress, which acts as a lubricant between the counter-sliding surfaces, resulting in ultra-low friction^[46]. Such phenomena were confirmed by MD simulations. In addition, friction process and mechanism of silver was also studied using TEM and electrostatic actuators in MEMS devices. The observed high strength and low separation forces are useful for understanding the frictional interactions^[73]. Lu *et al.* observed the frictional behavior of the silver-tungsten interface by means of TEM and Lorentz force-driven quantitative friction testing methods and found that the relative motion begins with plastic deformation of the silver, which will then transfer from static friction to dynamic friction^[114].

For the friction between covalently bonded materials, Hu *et al.* tested single-crystal Si, amorphous carbon and sp² nanocrystalline carbon through *in-situ* TEM nano-friction experiments and observed the formation of transfer films, which were found to stabilize the sliding process by decreasing the difference in stick-slip

friction coefficients^[115]. As shown in Figure 14C, by cleaving the atomic layers of MoS₂, the force between the layers was studied by the *in-situ* TEM technique^[116]. They found that the independent MoS₂ layers can easily slide and interlayer sliding may be limited by interactions with the probe. The ease of sliding was attributed to the low shear strength, which was reported to be only about 0.1 GPa. The superplastic behavior between Si asperities was also found by a TEM-MEMS technique induced by plastic deformation, decrystallization and atomic diffusion at the asperity interface.

Through *in-situ* TEM technology, the atomic structure of two surfaces can be observed and mechanical signals can be synchronously measured when friction occurs. The friction mechanism can be clarified at the atomic scale by analyzing the initial structure of the surface and the atomic movement paths during friction. In addition, by correlating the observed dynamic processes with the mechanical signals, it offers the possibility to quantitatively reveal the nature of the friction behavior.

FACTORS INFLUENCING THE MECHANICAL PROPERTIES OF NANOMATERIALS

Surface effect

As the size of the material shrinks, the surface area also increases, which greatly influences the mechanical properties of the material because the surface atoms have higher energies and lower coordination numbers. Typically, in terms of the elastic properties of a surface, whether it is stiffer or softer depends on the competition between hardening caused by the redistribution electrons of surface atoms and weakening due to the decrease in the coordination number on surface atoms^[29,84]. The influence of the surface on the elastic properties of a material is usually quantitatively analyzed by a core-shell model. For the plastic properties, the high surface energy makes it easier for defects such as dislocations to arise and escape during material deformation. Furthermore, recent studies have shown that surface atomic diffusion plays a non-negligible role in the plastic deformation of NMs.

To investigate the surface effect on Young's modulus of NMs with only a few nanometers thickness, a TEM experiment based on *in-situ* compression was used. As shown in Figure 15A, a significant increase in the Young's modulus was found for a sub-5nm thick amorphous Al₂O₃ layer, which is due to the reconstruction of the material's surface bonding and an increase in the surface-to-volume ratio with increasing nanoscale size^[117]. Similar to Al₂O₃, the Young's modulus of ZnO nanowires was found to increase with reducing size. Analysis by the core-shell model indicates that the surface layer has a higher Young's modulus, causing the size effect of the Young's modulus of the ZnO nanowires^[33,118].

In the case of metals, surface diffusion-assisted dislocation nucleation has been found by *in-situ* TEM techniques to lead to a transition in the strength-size dependence of Ag nanocrystals from a normal state to a Hall-Petch-like inversion^[119]. In addition, surface creep leads to anomalous softening of the Ag nanocrystals as the flow stress decreases with size, which is in contrast to the classical "alternating dislocation starvation" behavior of Pt nanocrystals [Figure 15B]. This study contributes to a deeper understanding of the mechanisms of diffusion-mediated atomic-scale deformation in nanoscale materials. Another competing factor affecting the deformation mechanism of single-crystal FCC metal nanowires, the shape of the cross-section, is reported by *in-situ* TEM tensile tests and MD simulations. In experiment, it is observed that twinning transfer to localized dislocation slip as the extent of truncation increases. Theoretical results also confirm the relationships between the twinning/dislocation slip energy barriers and the cross-sectional shape of the crystal. The energy barrier for twinning is proportional to the surface energy change caused by twinning. Therefore, the transition in the deformation mode is due to the change in surface energy, which is a function of the cross-sectional shape^[120]. Surface atom diffusion is also considered to be the key factor in reducing the Young's modulus of Au surface atoms, which reduced the total Young's modulus of Au nanocrystals^[22].

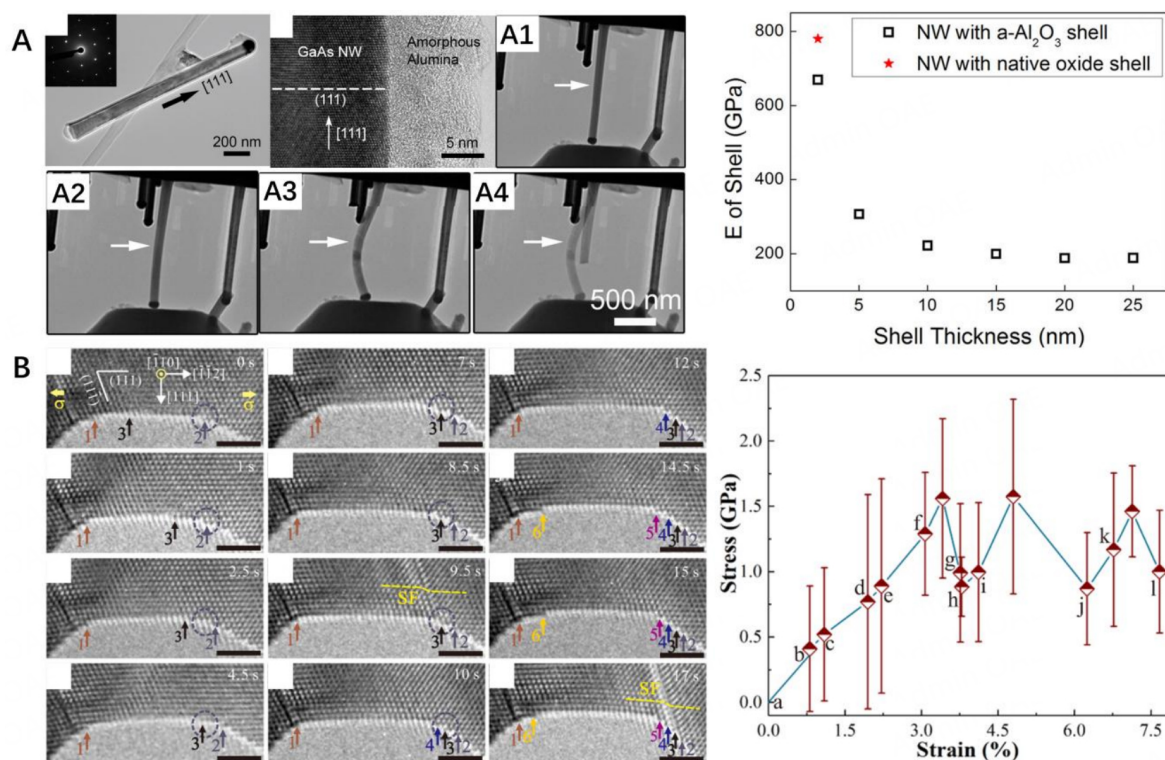


Figure 15. (A) Left: A series of microscopy images of a GaAs nanowire with a-Al₂O₃ shell before compression (A1), beginning of buckling (A2) and fracture point (A3 and A4). Right: Young's modulus of a-Al₂O₃ as a function of shell thickness. Reproduced with permission^[117]. Copyright 2015, ACS publications. (B) *In-situ* TEM study of surface diffusion-assisted dislocation nucleation in a Ga nanowire. Reproduced with permission^[119]. Copyright 2021, Springer Nature.

Defects

Defects, including point, line and surface defects, display an important role in the mechanical properties especially for NMs. For nanoscale materials, due to their small size, defect generation will significantly increase the defect density compared to bulk materials. The elastic modulus of 2D materials is reported to depend on defect concentration. In 2014, López-Polín *et al.* investigated the relationships between elasticity and strength of graphene versus defect concentration^[121]. They found the in-plane Young's modulus increases with increasing defect density up to almost twice the initial value for a vacancy content of ~0.2%, while for a higher density of vacancies, the elastic modulus decreases with defect inclusions. In addition, the fracture mechanism and strength of NMs is also related to the defects. The fracture process of nanoscale Mo single crystals, a BCC structure, contains the crack growth through the nucleation, motion, and interaction of dislocations on multiple $1/2 \langle 111 \rangle \{110\}$ slip systems at the crack tip^[122]. These dislocations resulted in the crack blunting, and localized segregation led to the crack extension and sharpening. Atomic simulations reveal the effects of temperature and strain rate on these alternating crack growth processes, providing insight into the mechanism of dislocation-mediated ductile-to-brittle transition in BCC metals. The movement of defects is also considered to be the driving force of the emerging viscoelastic behavior in NMs^[54]. Moreover, the influence of defects on the fracture strength of SiC nanowires from a few nanometres up to ~60 nm was also investigated by *in-situ* tensile tests. During experiment, the linear and elastic deformation process up to brittle fracture was observed. Figure 16A shows the occurrence of SF and twins in SiC nanowires during stretching. The fracture strength of SiC nanowires increased with decreasing nanowire diameter to more than 25 GPa, which is attributed to the dependence of size on defect density rather than to the main surface effect of single-crystal nanowires^[123].

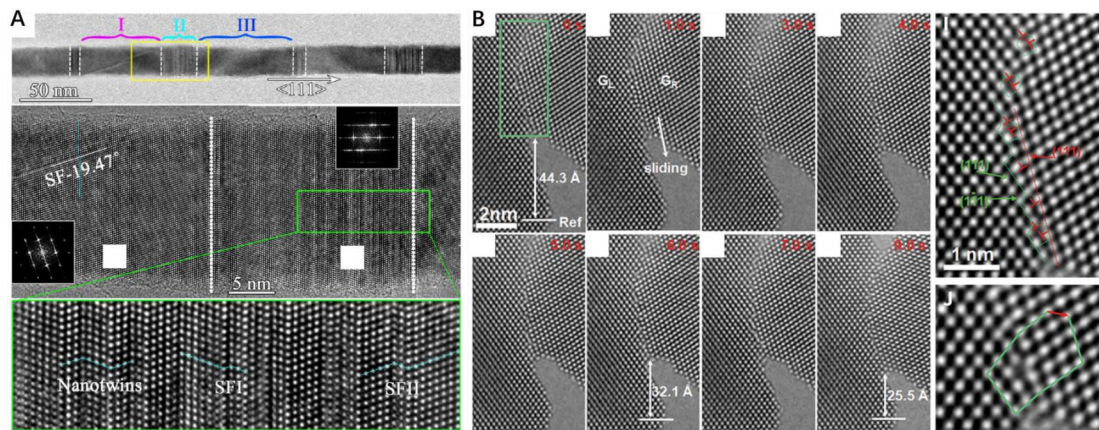


Figure 16. (A) TEM images of an individual SiC nanowire with SF and high-defective structures (nanotwins, intrinsic SFI, and extrinsic SFII). Reproduced with permission^[123]. Copyright 2014, ACS publications. (B) Atomic-scale sliding of an asymmetric tilt grain boundary in a Pt bicrystal. Reproduced with permission^[129]. Copyright 2022, The American Association for the Advancement of Science.

For metallic materials widely used in energy harvesting and storage, nanoelectromechanical devices, *etc.*, understanding how defects affect the deformation mechanism of metallic materials is also very important^[3,124,125]. *In-situ* tensile experiments under TEM revealed that Ag nanowires with a fivefold twin structure exhibit different behavior compared to single-crystalline ones. Upon loading, Ag nanowires with a fivefold twin structure undergo stress relaxation and then fully recover the plastic strain, which is not observed in single-crystal ones^[126]. For small crystals, plastic deformation is usually controlled by dislocation slip (full dislocation, partial dislocation, or winding). Yue *et al.* found that when the size of single-crystal nanowires is decreased to below 150 nm, the normal full dislocation slip is replaced by partial dislocation-mediated plasticity^[127]. Wang *et al.* found that for Pt nanocrystal sizes larger than 6 nm, the plastic deformation is mainly dislocation-dominated, but for sizes smaller than ~2 nm, dislocation-free plastic deformation dominates and a size dependence of dislocation activities was found^[128].

The *in-situ* TEM mechanics technique can also reflect the atomic-scale mechanisms of mechanical properties in bulk materials by observing the defect motion of the material at the atomic scale and guide the preparation of bulk materials. As shown in Figure 16B, recent *in-situ* atomic resolution TEM studies have shown that the dynamic deformation process at GBs is mainly accomplished by either direct sliding along the GBs at the atomic scale or sliding in the boundary plane as the atoms migrate^[129]. The atom transfer process is a previously unrecognized mode of GB sliding and atom plane transfer coupling. Bylinskii *et al.* measured the spring constant and sliding dissipation energy of Au nanocontacts with diameters of a few nanometres and estimated the critical shear stress (CSS) along the [112] direction using a quartz LER as the FM-AFM force sensor in both the elastic and plastic regions. Results show a relationship between the spring constant of the Au nanocontact and the amplitude of the LER; the value of CSS is measured to be about 0.94 GPa^[130].

Electric field

The external electric field may strongly affect the mechanical properties of NMs. The atoms may migrate under the external electrical field, driven by the electron wind force^[40,131]. Using *in-situ* TEM-STM techniques, Zhong *et al.* found that under an ultrafast electric pulse, the pure tantalum was successfully vitrified to form metallic glasses, as shown in Figure 17A^[132]. The cooling rate was estimated to be 1,014 K/s, which is considered to be the main factor of vitrification. The formation of monatomic metallic glasses provides novel opportunities for investigating its structural dependence of electrical, rheological and

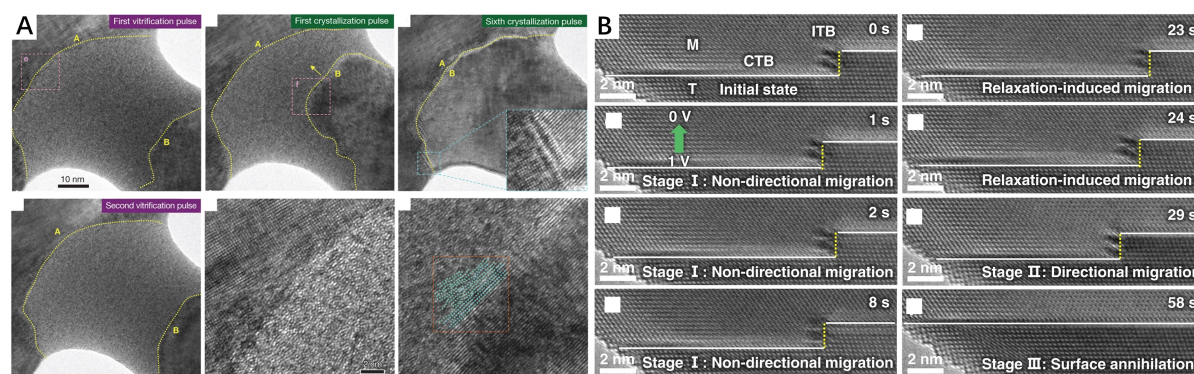


Figure 17. (A) A series of TEM images which show a vitrification-crystallization cycle in a tantalum sample when applying two electrical pulses with different voltages. Reproduced with permission^[132]. Copyright 2014, Springer Nature. (B) The surface annihilation of $\Sigma 3\{112\}$ 1 TB in Au nanocrystal under the continuous electrical pulses. Reproduced with permission^[135]. Copyright 2022, Springer Nature.

mechanical properties. Recently, a similar phenomenon of electric pulse-induced vitrification has been found in nanoscale zirconium and iridium^[133,134]. As shown in Figure 17B, Li *et al.* investigated the defect dynamics in Au nanocrystals under the electric pulse. Upon electropulsing, $\Sigma 3\{112\}$ incoherent twin boundaries (ITBs) were stimulated to migrate and the migration was independent of the electron direction. This is in contrast to the widely-held belief of directional atom migration under an external electric field. They demonstrate that the non-directional migration of ITBs was mainly affected by the interaction between electrons and dislocations instead of being driven by electron wind force^[135]. *In-situ* TEM tensile tests with a PTP device were performed on the single-crystal nickel nanowires by Li *et al.*, and the influence of applied mechanical and electrical fields on their nanostructure was observed^[136]. Based on their observations, the application of electric pulse results in a more homogeneous deformation than purely mechanically induced plasticity. They suggest that the electron wind force-induced enhancement of surface nucleation is more likely than Joule heating to account for the observed uniform plasticity during electrical pulsing^[136]. Gao *et al.* used *in-situ* TEM to quantitatively analyze the sensing mechanism of the graphite flakes. Their results demonstrate the critical roles played by the intrinsic deformation-induced current change of graphite flakes in enhancing the sensitivity. Their advanced *in-situ* electromechanical characterization of graphite flakes and experiment on devices reveals that the graphite flakes could be used in wearable sensors^[137].

SUMMARY AND OUTLOOK

Our review shows that *in-situ* TEM technology plays an irreplaceable role in studying the mechanical properties of materials due to its atomic-scale resolution and abundant information in the reciprocal space and energy space. In recent years, *in-situ* TEM technology has considerably developed, attributed to the recent advances in TEM imaging techniques, such as the development of aberration correctors, which have improved the spatial resolution of TEM^[4,74]. In addition, continually improving *in-situ* technologies are essential for obtaining high-quality TEM images and mechanical data. Various advanced mechanical structures and MEMS-based devices have been developed. They not only improve the stability of the sample, which could enhance the imaging resolution, but also enable the mechanical signal measurement.

It should be noted that mechanical testing with *in-situ* TEM is developing rapidly. The current *in-situ* mechanical TEM techniques still have great potential for further enhancement. (I) Although current *in-situ* TEM techniques and devices can well observe the deformation process of NMs and can measure the force signals during the deformation process, there is still potential to improve the resolution and accuracy of the

currently measured force signals, which can be achieved using more advanced mechanical sensors and more optimized circuit designs^[51,66]. Better quality force signals will allow researchers to conduct more precise quantitative analyses that can quantify the mechanical behavior of a material during deformation, such as the force and energy required to deform the material; (II) Compared to the excellent spatial resolution of spherical aberration TEM, the temporal resolution of *in-situ* TEM techniques is limited, especially in the case of *in-situ* three-dimension dislocation observation of NMs, which are severely constrained by the necessary mechanical tilting and the complexity of the autofocus and tracking process. Employing a direct electronic detection camera or combining MD simulation results may be a possible way to solve the above problem; (III) Besides, during the deformation of some alloys and compounds, the evolution of the chemical composition and structure will occur simultaneously. Energy dispersive X-ray spectroscopy (EDS) and electron energy loss spectroscopy (EELS) are two important techniques used to capture chemical information^[138,139]. Simultaneously detecting structural and chemical evolution during *in-situ* TEM deformation requires concurrent image capture and analysis of chemical composition. Advanced EDS and EELS detectors will facilitate the simultaneous acquisition of images and spectral data under *in-situ* deformation conditions; (IV) In addition, *in-situ* TEM results typically generate a large amount of data, especially videos taken during *in-situ* studies and mechanical signals corresponding to the material structure in the video. Scientists need to correlate the structural information with the corresponding force information to find the intrinsic connection, which undoubtedly requires a lot of efforts. Machine learning or artificial intelligence will provide crucial help in processing such large amounts of data, which is still little explored in the field; (V) Furthermore, some scientists have attempted to apply the results of *in-situ* TEM mechanical tests to the mechanical behavior of bulk materials. However, the specimens used in *in-situ* TEM deformation were at the micron or nanoscale, and the influence of crystal structure, orientation and surface conditions of the samples on defect nucleation and defect migration only applies to materials at the nanoscale. Therefore, relating the microscopic properties observed by *in-situ* TEM to the actual mechanical properties in bulk specimens remains to be urgently addressed; (VI) Current *in-situ* TEM techniques can only apply one or two external fields (e.g., force and electric fields), while the actual working environment of materials is often more complex. Therefore, it is often necessary to couple multiple external fields to simulate the actual working conditions of the material, in order to better combine the measured results with the reality. As the space for TEM samples is very limited, introducing multiple composite external fields (e.g., optical, electric, thermal, *etc.*) into the narrow space of TEM to investigate the mechanical properties of materials under complex external field conditions has attracted extensive interest from researchers. Future multi-field coupled *in situ* TEM technology may require not only special *in-situ* TEM holders but also the transformation of TEM columns to meet the purpose of multi-field measurement; and (VII) Measuring the mechanical properties at low temperatures is still very challenging even in the liquid nitrogen temperature range.

In conclusion, studying the mechanical properties of NMs by *in-situ* TEM will provide new insights into the structure-property-mechanism interactions of materials. By exploiting the high spatial resolution of TEM, *in-situ* TEM will provide an irreplaceable capability to reveal the atomic-scale dynamic processes of materials under deformation. In addition, the high energy resolution of TEM can be utilized to obtain important information on the elemental and compositional distribution of materials through EDS and EELS techniques. We believe that as *in-situ* TEM continues to develop, an increasing number of important nanomechanics results will be discovered.

DECLARATIONS

Authors' contributions

Supervision, conceptualization, validation, project administration, funding acquisition: Shan C, Cheng S, Zhang J

Original draft preparation, reviewing, and editing: Liu C, Zhang J, Yang K

Availability of data and materials

Not applicable.

Financial support and sponsorship

This work was supported by the National Natural Science Foundation of China (Grant No. 12304050 and No. 62271450), China Postdoctoral Science Foundation (Grant No. 2023M743227) and Natural Science Foundation of Henan Province (Grant No. 242300421669).

Conflicts of interest

Shaobo Cheng is an Editorial Board member of the journal *Microstructures*, while the other authors have declared that they have no conflicts of interest.

Ethical approval and consent to participate

Not applicable.

Consent for publication

Not applicable.

Copyright

© The Author(s) 2024.

REFERENCES

1. Gil-Santos E, Ramos D, Martínez J, et al. Nanomechanical mass sensing and stiffness spectrometry based on two-dimensional vibrations of resonant nanowires. *Nat Nanotechnol* 2010;5:641-5. [DOI](#)
2. Terabe K, Hasegawa T, Nakayama T, Aono M. Quantized conductance atomic switch. *Nature* 2005;433:47-50. [DOI](#) [PubMed](#)
3. Lord AM, Ramasse QM, Kepaptsoglou DM, Periwal P, Ross FM, Wilks SP. Stability of schottky and ohmic Au nanocatalysts to ZnO nanowires. *Nano Lett* 2017;17:6626-36. [DOI](#) [PubMed](#)
4. Cui L, Jeong W, Hur S, et al. Quantized thermal transport in single-atom junctions. *Science* 2017;355:1192-5. [DOI](#)
5. Jalabert L, Sato T, Ishida T, Fujita H, Chalopin Y, Volz S. Ballistic thermal conductance of a lab-in-a-TEM made Si nanojunction. *Nano Lett* 2012;12:5213-7. [DOI](#) [PubMed](#)
6. Smogunov A, Dal Corso A, Delin A, Weht R, Tosatti E. Colossal magnetic anisotropy of monatomic free and deposited platinum nanowires. *Nat Nanotechnol* 2008;3:22-5. [DOI](#) [PubMed](#)
7. Fernández-rossier J, Jacob D, Untiedt C, Palacios JJ. Transport in magnetically ordered Pt nanocontacts. *Phys Rev B* 2005;72:224418. [DOI](#)
8. Spataru CD, Ismail-Beigi S, Benedict LX, Louie SG. Excitonic effects and optical spectra of single-walled carbon nanotubes. *Phys Rev Lett* 2004;92:077402. [DOI](#) [PubMed](#)
9. Strasser P, Koh S, Anniyev T, et al. Lattice-strain control of the activity in dealloyed core-shell fuel cell catalysts. *Nat Chem* 2010;2:454-60. [DOI](#)
10. Strigl F, Espy C, Bückle M, Scheer E, Pietsch T. Emerging magnetic order in platinum atomic contacts and chains. *Nat Commun* 2015;6:6172. [DOI](#) [PubMed](#) [PMC](#)
11. Ma X, Zhao X, Wang T. Effect of strain on the electronic and magnetic properties of an Fe-doped WSe₂ monolayer. *RSC Adv* 2016;6:69758-63. [DOI](#)
12. Cai X, Niu C, Wang J, Yu W, Ren X, Zhu Z. Magnetic engineering in 3D transition metals on phosphorene by strain. *Phys Lett A* 2017;381:1236-40. [DOI](#)
13. Jiang C, Yang Z, Xiong W, Wang F. Effect of strain engineering on magnetism-induced valley splitting in WSe₂ based on the WSe₂/CrSe₂ heterojunction. *Appl Phys Lett* 2021;119:162101. [DOI](#)
14. Yi B, Pang R, Ren X, et al. Phase transition of nanoscale Au atom chains on NiAl(110). *Phys Lett A* 2020;384:126183. [DOI](#)
15. Li SF, Li H, Xue X, et al. Hcp metal nanoclusters with hexagonal A-A bilayer stacking stabilized by enhanced covalent bonding. *Phys Rev B* 2010;82:035443. [DOI](#)
16. Wang J, Wang L, Li Y, et al. Pressure-induced metallization of lead-free halide double perovskite (NH₄)₂PtI₆. *Adv Sci* 2022;9:e2203442. [DOI](#) [PubMed](#) [PMC](#)
17. Meyers MA, Chawla KK. Mechanical behavior of materials. Cambridge University Press; 2008. pp. 154-96. Available from: <https://>

- ceimusb.wordpress.com/wp-content/uploads/2015/04/mechanicalbehaviormeyers.pdf [Last accessed on 17 Jun 2023].
18. Lagos MJ, Sato F, Galvão DS, Ugarte D. Mechanical deformation of nanoscale metal rods: when size and shape matter. *Phys Rev Lett* 2011;106:055501. [DOI](#) [PubMed](#)
 19. Yang Y, Zhao C, Bai S, Wang C, Niu C. Activating MoS₂ basal planes for hydrogen evolution through the as doping and strain. *Phys Lett A* 2019;383:2997-3000. [DOI](#)
 20. Jiang C, Xiong W, Li C, Niu C, Wang F. Uniaxial strain induced symmetry lowering and valleys drift in MoS₂. *New J Phys* 2021;23:053007. [DOI](#)
 21. Kong D, Xin T, Sun S, et al. Surface energy driven liquid-drop-like pseudoelastic behaviors and in situ atomistic mechanisms of small-sized face-centered-cubic metals. *Nano Lett* 2019;19:292-8. [DOI](#)
 22. Zhang J, Tomitori M, Arai T, Oshima Y. Surface effect on Young's modulus of sub-two-nanometer gold [111] nanocontacts. *Phys Rev Lett* 2022;128:146101. [DOI](#) [PubMed](#)
 23. Diao J, Gall K, Dunn ML. Surface-stress-induced phase transformation in metal nanowires. *Nat Mater* 2003;2:656-60. [DOI](#) [PubMed](#)
 24. Tosatti E, Prestipino S, Kostlmeier S, Dal Corso A, Di Tolla FD. String tension and stability of magic tip-suspended nanowires. *Science* 2001;291:288-90. [DOI](#) [PubMed](#)
 25. Calvo MR, Sabater C, Dednam W, Lombardi EB, Caturla MJ, Untiedt C. Influence of relativistic effects on the contact formation of transition metals. *Phys Rev Lett* 2018;120:076802. [DOI](#) [PubMed](#)
 26. Wang Y, Li M, Xu J. Mechanical properties of spinodal decomposed metallic glass composites. *Scr Mater* 2017;135:41-5. [DOI](#)
 27. Tavazza F, Smith DT, Levine LE, Pratt JR, Chaka AM. Electron transport in gold nanowires: stable 1-, 2- and 3-dimensional atomic structures and noninteger conduction states. *Phys Rev Lett* 2011;107:126802. [DOI](#) [PubMed](#)
 28. Weinberger CR, Cai W. Plasticity of metal nanowires. *J Mater Chem* 2012;22:3277-92. [DOI](#)
 29. Zhou LG, Huang H. Are surfaces elastically softer or stiffer? *Appl Phys Lett* 2004;84:1940-2. [DOI](#)
 30. Fujii A, Tsutsui M, Kurokawa S, Sakai A. Break conductance of noble metal contacts. *Phys Rev B* 2005;72:045407. [DOI](#)
 31. Ternes M, González C, Lutz CP, et al. Interplay of conductance, force, and structural change in metallic point contacts. *Phys Rev Lett* 2011;106:016802. [DOI](#)
 32. Ternes M, Lutz CP, Hirjibehedin CF, Giessibl FJ, Heinrich AJ. The force needed to move an atom on a surface. *Science* 2008;319:1066-9. [DOI](#) [PubMed](#)
 33. Xu F, Qin Q, Mishra A, Gu Y, Zhu Y. Mechanical properties of ZnO nanowires under different loading modes. *Nano Res* 2010;3:271-80. [DOI](#)
 34. Wu B, Heidelberg A, Boland JJ. Mechanical properties of ultrahigh-strength gold nanowires. *Nat Mater* 2005;4:525-9. [DOI](#) [PubMed](#)
 35. Hoffmann S, Utke I, Moser B, et al. Measurement of the bending strength of vapor-liquid-solid grown silicon nanowires. *Nano Lett* 2006;6:622-5. [DOI](#)
 36. Comtet J, Lainé A, Niguès A, Bocquet L, Siria A. Atomic rheology of gold nanojunctions. *Nature* 2019;569:393-7. [DOI](#) [PubMed](#)
 37. Canale L, Comtet J, Niguès A, et al. Nanorheology of interfacial water during ice gliding. *Phys Rev X* 2019;9:041025. [DOI](#)
 38. Khosravi A, Lainé A, Vanossi A, Wang J, Siria A, Tosatti E. Understanding the rheology of nanocontacts. *Nat Commun* 2022;13:2428. [DOI](#) [PubMed](#) [PMC](#)
 39. Shiota T, Mares AI, Valkering AMC, Oosterkamp TH, van Ruitenbeek JM. Mechanical properties of Pt monatomic chains. *Phys Rev B* 2008;77:125411. [DOI](#)
 40. Oshima Y, Kurui Y. In situ TEM observation of controlled gold contact failure under electric bias. *Phys Rev B* 2013;87:081404. [DOI](#)
 41. Kondo Y, Takayanagi K. Synthesis and characterization of helical multi-shell gold nanowires. *Science* 2000;289:606-8. [DOI](#) [PubMed](#)
 42. Wang L, Liu P, Guan P, et al. In situ atomic-scale observation of continuous and reversible lattice deformation beyond the elastic limit. *Nat Commun* 2013;4:2413. [DOI](#) [PubMed](#) [PMC](#)
 43. Zhang H, Tersoff J, Xu S, et al. Approaching the ideal elastic strain limit in silicon nanowires. *Sci Adv* 2016;2:e1501382. [DOI](#) [PubMed](#) [PMC](#)
 44. Nie A, Bu Y, Li P, et al. Approaching diamond's theoretical elasticity and strength limits. *Nat Commun* 2019;10:5533. [DOI](#) [PubMed](#) [PMC](#)
 45. Kiener D, Minor AM. Source truncation and exhaustion: insights from quantitative in situ TEM tensile testing. *Nano Lett* 2011;11:3816-20. [DOI](#) [PubMed](#) [PMC](#)
 46. He Y, She D, Liu Z, et al. Atomistic observation on diffusion-mediated friction between single-asperity contacts. *Nat Mater* 2022;21:173-80. [DOI](#)
 47. Dang C, Chou JP, Dai B, et al. Achieving large uniform tensile elasticity in microfabricated diamond. *Science* 2021;371:76-8. [DOI](#)
 48. Liu P, Wei X, Song S, et al. Time-resolved atomic-scale observations of deformation and fracture of nanoporous gold under tension. *Acta Mater* 2019;165:99-108. [DOI](#)
 49. Guo H, Chen K, Oh Y, et al. Mechanics and dynamics of the strain-induced M1-M2 structural phase transition in individual VO₂ nanowires. *Nano Lett* 2011;11:3207-13. [DOI](#)
 50. Chen Y, Liao X. Chapter Four - Mechanical behaviors of semiconductor nanowires. *Semicond Semimet* 2016;94:109-58. [DOI](#)
 51. Lu Y, Song J, Huang JY, Lou J. Fracture of sub-20 nm ultrathin gold nanowires. *Adv Funct Mater* 2011;21:3982-9. [DOI](#)
 52. Sun S, Kong D, Li D, et al. Atomistic mechanism of stress-induced combined slip and diffusion in sub-5 nanometer-sized Ag nanowires. *ACS Nano* 2019;13:8708-16. [DOI](#)

53. Wang X, Liu Z, He Y, Tan S, Wang G, Mao SX. Atomic-scale friction between single-asperity contacts unveiled through in situ transmission electron microscopy. *Nat Nanotechnol* 2022;17:737-45. [DOI](#)
54. Cheng G, Miao C, Qin Q, et al. Large anelasticity and associated energy dissipation in single-crystalline nanowires. *Nat Nanotechnol* 2015;10:687-91. [DOI](#)
55. Moresco F. Manipulation of large molecules by low-temperature STM: model systems for molecular electronics. *Phys Rep* 2004;399:175-225. [DOI](#)
56. Svensson K, Jompol Y, Olin H, Olsson E. Compact design of a transmission electron microscope-scanning tunneling microscope holder with three-dimensional coarse motion. *Rev Sci Instrum* 2003;74:4945-7. [DOI](#)
57. Kawamoto N, Kakefuda Y, Yamada I, et al. Visualizing nanoscale heat pathways. *Nano Energy* 2018;52:323-8. [DOI](#)
58. Oshima Y, Mouri K, Hirayama H, Takayanagi K. Development of a miniature STM holder for study of electronic conductance of metal nanowires in UHV-TEM. *Surf Sci* 2003;531:209-16. [DOI](#)
59. Oshima Y, Koizumi H, Mouri K, Hirayama H, Takayanagi K, Kondo Y. Evidence of a single-wall platinum nanotube. *Phys Rev B* 2002;65:121401. [DOI](#)
60. Xu M, Dai S, Blum T, Li L, Pan X. Double-tilt in situ TEM holder with ultra-high stability. *Ultramicroscopy* 2018;192:1-6. [DOI](#)
61. Gibson CT, Weeks BL, Abell C, Rayment T, Myhra S. Calibration of AFM cantilever spring constants. *Ultramicroscopy* 2003;97:113-8. [DOI](#) [PubMed](#)
62. Nafari A, Karlen D, Rusu C, Svensson K, Olin H, Enoksson P. MEMS sensor for *in situ* TEM atomic force microscopy. *J Microelectromech Syst* 2008;17:328-33. [DOI](#)
63. Giessibl FJ, Pielmeier F, Eguchi T, An T, Hasegawa Y. Comparison of force sensors for atomic force microscopy based on quartz tuning forks and length-extensional resonators. *Phys Rev B* 2011;84:125409. [DOI](#)
64. An T, Eguchi T, Akiyama K, Hasegawa Y. Atomically-resolved imaging by frequency-modulation atomic force microscopy using a quartz length-extension resonator. *Appl Phys Lett* 2005;87:133114. [DOI](#)
65. Giessibl FJ. Advances in atomic force microscopy. *Rev Mod Phys* 2003;75:949-83. [DOI](#)
66. Zhang J, Ishizuka K, Tomitori M, Arai T, Oshima Y. Atomic scale mechanics explored by in situ transmission electron microscopy with a quartz length-extension resonator as a force sensor. *Nanotechnology* 2020;31:205706. [DOI](#) [PubMed](#)
67. Wang L, Guan P, Teng J, et al. New twinning route in face-centered cubic nanocrystalline metals. *Nat Commun* 2017;8:2142. [DOI](#) [PubMed](#) [PMC](#)
68. Wang L, Teng J, Sha X, Zou J, Zhang Z, Han X. Plastic deformation through dislocation saturation in ultrasmall Pt nanocrystals and its in situ atomistic mechanisms. *Nano Lett* 2017;17:4733-9. [DOI](#) [PubMed](#)
69. Mompou F, Legros M. Quantitative grain growth and rotation probed by in-situ TEM straining and orientation mapping in small grained Al thin films. *Scr Mater* 2015;99:5-8. [DOI](#)
70. Xie L, Oshima Y. Nonlinear mechanical response of rippled MoS₂ nanosheets evaluated by in situ transmission electron microscopy. *Appl Surf Sci* 2022;597:153708. [DOI](#)
71. Zhu Y, Espinosa HD. An electromechanical material testing system for in situ electron microscopy and applications. *Proc Natl Acad Sci USA* 2005;102:14503-8. [DOI](#) [PubMed](#) [PMC](#)
72. Sato T, Ishida T, Jalabert L, Fujita H. Real-time transmission electron microscope observation of nanofriction at a single Ag asperity. *Nanotechnology* 2012;23:505701. [DOI](#)
73. Sato T, Milne ZB, Nomura M, Sasaki N, Carpick RW, Fujita H. Ultrahigh strength and shear-assisted separation of sliding nanocontacts studied in situ. *Nat Commun* 2022;13:2551. [DOI](#) [PubMed](#) [PMC](#)
74. Zhang J, Li Y, Li X, et al. Timely and atomic-resolved high-temperature mechanical investigation of ductile fracture and atomistic mechanisms of tungsten. *Nat Commun* 2021;12:2218. [DOI](#) [PubMed](#) [PMC](#)
75. Nie A, Bu Y, Huang J, et al. Direct observation of room-temperature dislocation plasticity in diamond. *Matter* 2020;2:1222-32. [DOI](#)
76. Chen Y, An X, Liao X. Mechanical behaviors of nanowires. *Appl Phys Rev* 2017;4:031104. [DOI](#)
77. Zhu Y, Qin Q, Xu F, et al. Size effects on elasticity, yielding, and fracture of silver nanowires: *in situ* experiments. *Phys Rev B* 2012;85:045443. [DOI](#)
78. Feng G, Nix WD, Yoon Y, Lee CJ. A study of the mechanical properties of nanowires using nanoindentation. *J Appl Phys* 2006;99:074304. [DOI](#)
79. Dai S, Zhao J, He MR, et al. Elastic properties of GaN nanowires: revealing the influence of planar defects on young's modulus at nanoscale. *Nano Lett* 2015;15:8-15. [DOI](#)
80. Chen Y, Burgess T, An X, et al. Effect of a high density of stacking faults on the Young's modulus of GaAs nanowires. *Nano Lett* 2016;16:1911-6. [DOI](#)
81. Wang YB, Wang LF, Joyce HJ, et al. Super deformability and Young's modulus of GaAs nanowires. *Adv Mater* 2011;23:1356-60. [DOI](#)
82. Liu C, Hongo K, Maezono R, Zhang J, Oshima Y. Stiffer bonding of armchair edge in single-layer molybdenum disulfide nanoribbons. *Adv Sci* 2023;10:e2303477. [DOI](#) [PubMed](#) [PMC](#)
83. Cammarata RC. Surface and interface stress effects in thin films. *Prog Surf Sci* 1994;46:1-38. [DOI](#)
84. Cuenot S, Frétygny C, Demoustier-champagne S, Nysten B. Surface tension effect on the mechanical properties of nanomaterials measured by atomic force microscopy. *Phys Rev B* 2004;69:165410. [DOI](#)
85. Zhang J, Ishizuka K, Tomitori M, et al. Peculiar atomic bond nature in platinum monatomic chains. *Nano Lett* 2021;21:3922-8. [DOI](#)

86. Li D, Wang Z, Zhao Y, et al. In situ atomic-scale quantitative evidence of plastic activities resulting in reparable deformation in ultrasmall-sized Ag nanocrystals. *ACS Nano* 2023;17:23488-97. DOI
87. Östlund F, Rzepiejewska-Malyska K, Leifer K, et al. Brittle-to-ductile transition in uniaxial compression of silicon pillars at room temperature. *Adv Funct Mater* 2009;19:2439-44. DOI
88. Wang L, Zheng K, Zhang Z, Han X. Direct atomic-scale imaging about the mechanisms of ultralarge bent straining in Si nanowires. *Nano Lett* 2011;11:2382-5. DOI
89. Zheng X, Han W, Yang K, et al. Phase and polarization modulation in two-dimensional In_2Se_3 via in situ transmission electron microscopy. *Sci Adv* 2022;8:eabo0773. DOI PubMed PMC
90. Seo JH, Park HS, Yoo Y, et al. Origin of size dependency in coherent-twin-propagation-mediated tensile deformation of noble metal nanowires. *Nano Lett* 2013;13:5112-6. DOI
91. Chu S, Liu P, Zhang Y, et al. In situ atomic-scale observation of dislocation climb and grain boundary evolution in nanostructured metal. *Nat Commun* 2022;13:4151. DOI PubMed PMC
92. Wang J, Sansoz F, Huang J, et al. Near-ideal theoretical strength in gold nanowires containing angstrom scale twins. *Nat Commun* 2013;4:1742. DOI PubMed PMC
93. Zhu Q, Huang Q, Guang C, et al. Metallic nanocrystals with low angle grain boundary for controllable plastic reversibility. *Nat Commun* 2020;11:3100. DOI PubMed PMC
94. Yang C, Zhang B, Fu L, et al. Chemical inhomogeneity-induced profuse nanotwinning and phase transformation in AuCu nanowires. *Nat Commun* 2023;14:5705. DOI PubMed PMC
95. Fu L, Yang C, Lu Y, et al. In situ atomistic mechanisms of detwinning in nanocrystalline AuAg alloy. *Sci China Mater* 2022;65:820-6. DOI
96. Chen B, Gao Q, Wang Y, et al. Anelastic behavior in GaAs semiconductor nanowires. *Nano Lett* 2013;13:3169-72. DOI
97. Sheng H, Zheng H, Cao F, et al. Anelasticity of twinned CuO nanowires. *Nano Res* 2015;8:3687-93. DOI
98. Sun J, He L, Lo YC, et al. Liquid-like pseudoelasticity of sub-10-nm crystalline silver particles. *Nat Mater* 2014;13:1007-12. DOI
99. Wang J, Zeng Z, Weinberger CR, Zhang Z, Zhu T, Mao SX. In situ atomic-scale observation of twinning-dominated deformation in nanoscale body-centred cubic tungsten. *Nat Mater* 2015;14:594-600. DOI
100. Li L, Chen G, Zheng H, et al. Room-temperature oxygen vacancy migration induced reversible phase transformation during the anelastic deformation in CuO. *Nat Commun* 2021;12:3863. DOI PubMed PMC
101. Huang L, Zheng F, Deng Q, et al. In situ scanning transmission electron microscopy observations of fracture at the atomic scale. *Phys Rev Lett* 2020;125:246102. DOI
102. Ly TH, Zhao J, Cichocka MO, Li LJ, Lee YH. Dynamical observations on the crack tip zone and stress corrosion of two-dimensional MoS_2 . *Nat Commun* 2017;8:14116. DOI PubMed PMC
103. Wang S, Qin Z, Jung GS, et al. Atomically sharp crack tips in monolayer MoS_2 and their enhanced toughness by vacancy defects. *ACS Nano* 2016;10:9831-9. DOI
104. López-Polín G, Gómez-Herrero J, Gómez-Navarro C. Confining crack propagation in defective graphene. *Nano Lett* 2015;15:2050-4. DOI PubMed
105. Qiu K, Hou J, Chen S, et al. Self-healing of fractured diamond. *Nat Mater* 2023;22:1317-23. DOI
106. Wang Q, Liu K, Xue X, et al. Negative differential friction predicted in two-dimensional electride commensurate contacts: role of the electronic structure. *Phys Rev B* 2024;109:085420. DOI
107. Sun J, Zhang L, Pang R, et al. Negative differential friction predicted in 2D ferroelectric In_2Se_3 commensurate contacts. *Adv Sci* 2022;9:e2103443. DOI PubMed PMC
108. Cheng J, Liu K, Zhao X, et al. Negative-positive oscillation in interfacial friction of a In_2Se_3 -graphene heterojunction. *Phys Rev B* 2022;106:195416. DOI
109. Liu K, Cheng J, Zhao X, et al. Negative differential friction coefficients of two-dimensional commensurate contacts dominated by electronic phase transition. *Nano Res* 2022;15:5758-66. DOI
110. Chen C, Xue P, Fan X, Wang C, Diao D. Friction-induced rapid restructuring of graphene nanocrystallite cap layer at sliding surfaces: short run-in period. *Carbon* 2018;130:215-21. DOI
111. Guerra R, Tartaglino U, Vanossi A, Tosatti E. Ballistic nanofriction. *Nat Mater* 2010;9:634-7. DOI PubMed
112. Bylinskii A, Gangloff D, Counts I, Vuletić V. Observation of Aubry-type transition in finite atom chains via friction. *Nat Mater* 2016;15:717-21. DOI PubMed
113. Holmberg K, Erdemir A. Influence of tribology on global energy consumption, costs and emissions. *Friction* 2017;5:263-84. DOI
114. Lu H, Wang Z, Yun D, Li J, Shan Z. A new approach of using Lorentz force to study single-asperity friction inside TEM. *J Mater Sci Technol* 2021;84:43-8. DOI
115. Hu Z, Fan X, Diao D. Facilitation of sp^2 nanocrystallites on the formation of transfer films for stable low friction with in-situ TEM nanofriction study. *Tribol Int* 2022;174:107713. DOI
116. Tang DM, Kvashnin DG, Najmaei S, et al. Nanomechanical cleavage of molybdenum disulphide atomic layers. *Nat Commun* 2014;5:3631. DOI
117. Chen Y, Gao Q, Wang Y, et al. Determination of Young's modulus of ultrathin nanomaterials. *Nano Lett* 2015;15:5279-83. DOI
118. Chen CQ, Shi Y, Zhang YS, Zhu J, Yan YJ. Size dependence of Young's modulus in ZnO nanowires. *Phys Rev Lett* 2006;96:075505. DOI

119. Wang X, Zheng S, Shinzato S, et al. Atomistic processes of surface-diffusion-induced abnormal softening in nanoscale metallic crystals. *Nat Commun* 2021;12:5237. DOI PubMed PMC
120. Yin S, Cheng G, Richter G, Gao H, Zhu Y. Transition of deformation mechanisms in single-crystalline metallic nanowires. *ACS Nano* 2019;13:9082-90. DOI PubMed
121. López-polín G, Gómez-navarro C, Parente V, et al. Increasing the elastic modulus of graphene by controlled defect creation. *Nature Phys* 2015;11:26-31. DOI
122. Lu Y, Chen Y, Zeng Y, et al. Nanoscale ductile fracture and associated atomistic mechanisms in a body-centered cubic refractory metal. *Nat Commun* 2023;14:5540. DOI PubMed PMC
123. Cheng G, Chang TH, Qin Q, Huang H, Zhu Y. Mechanical properties of silicon carbide nanowires: effect of size-dependent defect density. *Nano Lett* 2014;14:754-8. DOI
124. Oshima Y, Kurui Y, Takayanagi K. Controlling quantized steps in conductance of gold Zigzag nanowires. *Appl Phys Express* 2011;4:055002. DOI
125. Wang Q, Liu R, Xiang D, et al. Single-atom switches and single-atom gaps using stretched metal nanowires. *ACS Nano* 2016;10:9695-702. DOI
126. Qin Q, Yin S, Cheng G, et al. Recoverable plasticity in penta-twinned metallic nanowires governed by dislocation nucleation and retraction. *Nat Commun* 2015;6:5983. DOI PubMed PMC
127. Yue Y, Liu P, Deng Q, Ma E, Zhang Z, Han X. Quantitative evidence of crossover toward partial dislocation mediated plasticity in copper single crystalline nanowires. *Nano Lett* 2012;12:4045-9. DOI PubMed
128. Wang L, Teng J, Wu Y, et al. Size dependence of dislocation activities and independence on theoretical elastic strain limit in Pt nanocrystals revealed by atomic-resolution in situ investigation. *Mater Today Nano* 2018;2:1-6. DOI
129. Wang L, Zhang Y, Zeng Z, et al. Tracking the sliding of grain boundaries at the atomic scale. *Science* 2022;375:1261-5. DOI
130. Liu J, Zhang J, Arai T, Tomitori M, Oshima Y. Critical shear stress of gold nanocontacts estimated by in situ transmission electron microscopy equipped with a quartz length-extension resonator. *Appl Phys Express* 2021;14:075006. DOI
131. Suzuki Y, Kizuka T. Structure control of tungsten nanocontacts through pulsed-voltage application. *Appl Phys Express* 2018;11:055202. DOI
132. Zhong L, Wang J, Sheng H, Zhang Z, Mao SX. Formation of monatomic metallic glasses through ultrafast liquid quenching. *Nature* 2014;512:177-80. DOI
133. Tsuruoka Y, Obi T, Kizuka T. Reversible phase-transition control in nanometer-sized zirconium wires via pulse-voltage impression. *Nano Express* 2020;1:010050. DOI
134. Obi T, Ochiai Y, Tsuruoka Y, Kizuka T. Amorphization of pure noble metal nanocontacts by nanosecond electrical energization. *J Phys Chem Solids* 2022;162:110498. DOI
135. Li X, Zhu Q, Hong Y, et al. Revealing the pulse-induced electroplasticity by decoupling electron wind force. *Nat Commun* 2022;13:6503. DOI PubMed PMC
136. Li X, Turner J, Bustillo K, Minor AM. In situ transmission electron microscopy investigation of electroplasticity in single crystal nickel. *Acta Mater* 2022;223:117461. DOI
137. Gao L, Cao K, Hu X, et al. Nano electromechanical approach for flexible piezoresistive sensor. *Appl Mater Today* 2020;18:100475. DOI
138. Tinoco M, Maduro L, Masaki M, Okunishi E, Conesa-Boj S. Strain-dependent edge structures in MoS₂ layers. *Nano Lett* 2017;17:7021-6. DOI PubMed PMC
139. Idrus-saidi SA, Tang J, Ghasemian MB, et al. Liquid metal core-shell structures functionalised via mechanical agitation: the example of Field's metal. *J Mater Chem A* 2019;7:17876-87. DOI